Translatomic database of cortical astroglia across male and female mouse development reveals two distinct developmental phenotypes

Gareth M. Rurak[1], Stephanie Simard[1], François Charih[4], Amanda Van Geel[1], John Stead[1], Barbara Woodside[1,3], James R. Green[4], Gianfilippo Coppola*[2], Natalina Salmaso*[1,2]

Running Title:

Affiliations: 1-Department of Neuroscience, Carleton University, Ottawa, Ontario;
2-Child Study Center, Yale University; 3- Concordia University, Montreal, Quebec
4-Department of Systems and Computer Engineering, Carleton University, Ottawa, Ontario

*co-corresponding authors

Authors for Correspondence:

Natalina Salmaso
Carleton University, 1125 Colonel By Drive, Ottawa, Ontario, K1S 5B6, Canada
Tel: 613-520 2600
Email: natalina.salmaso@carleton.ca

Gianfilippo Coppola
Yale University, 333 Cedar st, New Haven, CT 06511, USA
Email: gianfilippo.coppola@yale.edu

Abstract

Astroglial cells are emerging as key players in the development and homeostatic maintenance of neurons and neuronal networks. Astroglial cell functions are critical to neuronal migration and maturation, myelination, and synapse dynamics, however little is known about astroglial phenotypic changes over development. Furthermore, astroglial cells express steroid hormone receptors and show rapid responses to hormonal manipulations, however, despite important sex differences in telencephalic regions such as the cortex and hippocampus few studies have examined sex differences in astroglial cells in development and outside of the hypothalamus and amygdala. To phenotype cortical astroglial cells across postnatal development while considering potential sex differences, we used translating ribosome affinity purification together with RNA sequencing (TRAPseq) and immunohistochemistry to phenotype the entire astroglial translatome in males and females at key developmental time points: P1, P4, P7, P14, P35 and in adulthood. Overall, we found two distinct astroglial phenotypes between early (P1-P7) and late development (P14-Adult). We also noted that although astroglia show few basal sex differences in adulthood, they show significant sex differences in developmental gene expression patterns, with peak sex differences observed at P7. At least part of the sex differences observed at P7 appear to be due to males reaching a more mature astroglial phenotype earlier than females. Together, these data clearly delineate and phenotype astroglia across development and identify sex differences in astroglial developmental programs. Importantly, these developmental sex differences could have an impact on the construction and maintenance of neuronal networks and potential developmental windows of vulnerability to neurologic and psychiatric disease.

Acknowledgements

We would like to thank our funding providers, the Carleton University Discovery Grant to N.S., Natural Sciences and Engineering Research Council of Canada Discovery Grant to N.S., the Canadian Foundation for Innovation to N.S., and the Canadian Research Chairs to N.S..

We thank Dr. Julianna Tomlinson, Dr. Michael Schlossmacher and his laboratory members at the University of Ottawa for providing us with infrastructural support and more. Finally, we would like to thank Dr. Alfonso Abizaid for his invaluable input into the planning and preparation of this research project.

Introduction

The cerebral cortex is a complex network of layered neuronal cells that uses a balance of excitatory and inhibitory signals to communicate both within the cerebral cortex itself and to lower brain regions[1]. It is the most recently evolved component of the mammalian central nervous system and is uniquely involved in higher order cognitive functions[2] that are central to cognitive and emotional processing. The complex layered structure of the cerebral cortex emerges during embryonic development in an "inside-out" pattern consisting of radial glial cell (RGC)-assisted neuroblast migration to lower layers (i.e. VI) before the upper layers are formed [3,4]. The appropriate migration of developing neuroblasts is an integral part of the maturation of the cerebral cortex. Early insults or perturbations during this critical period of development may disrupt the gross organization of excitatory and inhibitory networks leading to neurodevelopmental disorders including autism spectrum disorders (ASD), schizophrenia, and mood disorders such as bipolar disorder[5,6]. Importantly, even subtle modifications in the number or functionality of cortical synapses may lead to serious behavioural consequences and have been related to a number of psychiatric diseases[7].

In human populations the prevalence of many, if not all, neurodevelopmental disorders and mood disorders related to cortical function is dependent on sex [8] .Thus understanding sex differences in the organization and function of the cerebral cortex is critical to understanding the neurodevelopmental underpinnings of psychiatric disease. There is a great deal of literature that suggests that gonadal hormones can directly modulate disease states associated with schizophrenia, anxiety and mood disorders[9,10]. Similarly, in rodent models, basal changes in behaviours such as in the forced swim task have been demonstrated across the estrous cycle[11]. Together, these data support an important role for ovarian hormones and in particular, estrogen, in mediating those behaviours related to higher order cognitive functioning in situ. Effects on behaviour and physiology that depend on current levels of hormones such as those described above are referred to as activational. The sex steroid milieu of embryonic and neonatal life, however, can also have organizational effects. These are changes induced in this early stage of development that persist even when the hormonal state producing them has dissipated.

90 Testosterone secreted from the testes of XY-male embryos acting either directly or via
91 aromatisation to estradiol is the primary organizing influence in the sexual differentiation
92 of the brain[12,13]; The role of estradiol in mediating organizational sex differences through
93 neuronal estrogen receptor (ERs) signaling has been extensively studied in the
94 hypothalamus and amygdala. For example, in the medial pre-optic area (MPOA),
95 estrogen receptor signalling induces prostaglandin-mediated synapse formation through
96 microglial and astroglial-mediated functions[13]. Neuroanatomical and functional sex
97 differences are also well defined in various neuronal populations of the hypothalamus[14],
98 amygdala[15], and hippocampus[16]. The cerebral cortex, however, has received less
99 attention than other telencephalic regions[17].

100 While it is possible that sex differences in cortical network functioning may be
101 completely mediated by direct hormonal modulation, sex differences in the prevalence of
102 anxiety disorders[9] and ASD[18] are apparent prior to puberty, and pro-dromal behaviours
103 associated with psychosis also show sex differences early in development[19], suggesting
104 that organizational sex differences (presumably in cortical networks) may be involved in
105 differences in risk or vulnerability for psychiatric disease.

106 Astroglial cells have recently emerged as key mediators in brain development and
107 the etiology of neurodevelopmental and mood disorders has been related to astroglial-
108 mediated functions such as neuroblast migration and synapse formation, maturation, and
109 elimination[20,21]. Cortical astroglial cells are a heterogenous cell population traditionally
110 categorised into three main subtypes easily distinguished by morphology, although recent
111 work has suggested that many more subtypes exist when astroglial cells are categorised
112 through single cell RNAseq or other gene and protein expression methods[22,23]. The first
113 subtype of astroglial cells to emerge in development are RGCs[24]. In addition to providing
114 scaffolding for migrating neuroblasts, astroglial cells exhibit stem-like potential in early
115 development and following injury that allows them to give rise to other neuronal cells
116 before maturing and populating the cortex as fibrous or protoplasmic astroglial cells[25,26].
117 As astroglia mature, their stem cell potential diminishes, as marked by an increase in
118 glutamate synthetase and decreased expression of Sox2 and vimentin[27]. The two main
119 mature morphological subtypes in the cortex are characterized as protoplasmic; canonical

120 astroglia with large domains of many fine processes, and fibrous; astroglial cells with
121 many long fibrous extensions[28]. These mature astroglial cell populations are responsible
122 for the construction and maintenance of both excitatory[29] and inhibitory[30] synapses in the
123 developing neocortex, modulating neuron signaling and maturation[31], and the elimination
124 of synapses during cortical maturation[21]. Work from the Barres laboratory characterised
125 astroglial cells in brain development using next generation sequencing techniques,
126 however these studies did not examine the contributions of biological sex, or early
127 developmental periods[32]. Astroglial cells express ERα[33], ERβ[34], and G-protein coupled
128 ERs[35], and although the full extent of ER functionality in astroglial cells is not
129 understood[36], astroglia show rapid responses to hormones across various states and
130 manipulations[37].
131 Because astroglial cells contribute to cortical development through neuroblast
132 migration, neuronal network integration, and synapse formation, maturation and
133 elimination, and because astroglia show rapid responses to hormones, we hypothesized
134 that cortical astroglial cells may 1) show phenotypic sex differences both overall and
135 across development and 2) execute developmental functions in a sexually dimorphic way.
136 To address this, we employed a transgenic mouse model expressing enhanced green
137 fluorescent protein (eGFP) fused to the L10 ribosome under the pan-astroglial cell
138 promoter AldH-L1 and used immunohistochemistry and TRAPseq to phenotype the
139 astroglial translatome and protein expression. We examined time points pertaining to
140 critical periods of postnatal neocortical development.
141
142

143 Results

144 Our initial characterization of neocortical astroglial cells set to measure total
145 numbers of neocortical astroglial cells (astroglial cell number) across development in both
146 males and females. We used unbiased stereology to quantify eGFP+ cells (eGFP was
147 expressed under the control of the pan-astroglial promoter, AldH1l1). No sex differences
148 in total astroglial number were observed ($F_{1,41}$=0.716, p=0.402, $H\eta$=0.017) (Figure 1A),
149 however there was a main effect of age on this measure ($F_{5,41}$=58.313, p<0.001,
150 $H\eta$=0.874), whereby the number of astroglial cells plateaued in both males or females
151 after P14 (Figure 1A). Additionally, neocortical volume did not exhibit any significant
152 sexual dimorphism ($F_{1,41}$=0.009, p=0.923, $H\eta$=0) (Figure 1B). Not surprisingly, we
153 observed a significant increase of brain volume with age (($F_{5,41}$=135.181, p<0.001,
154 $H\eta$=0.943) (Figure 1B).

155 Astroglial cells show a great deal of morphological heterogeneity that are typically
156 associated with functionality (Sofroniew & Vinters, 2010). One difference in morphology
157 that is seen during cortical development is an early abundance of the radial phenotype
158 that is replaced by protoplasmic astroglia over development. We assessed gross
159 morphological changes in development (from radial to non-radial) across age to ascertain
160 whether sex differences exist. eGFP+ cells were characterized as radial or non-radial
161 based on the presence of a leading, radial process in the neocortex. No significant sex
162 effects were found ($F_{1,41}$=0.004, p=0.953, $H\eta$=0), however there was a significant effect
163 of age ($F_{5,41}$=89.291, p<0.001, $H\eta$=0.916) (Figure 1C). Nearly all (~95% in both males
164 and females) astroglial cells in the neocortex at P1 exhibited radial morphology (Figure
165 1C).

166 To generate a more complete characterization of neocortical astroglia over
167 development and in relation to sex, we employed TRAPseq to assess the astroglial-
168 specific translatome in males and females at each time point. Gene expression levels (as
169 RPKM) for all expressed genes can be found in our searchable database at http://cu-
170 bic.ca/stardb (see Methods). To validate our TRAPseq methodology, we used q-RT-PCR
171 to compare the unbound fragment to its bound counterpart on levels of two astroglial
172 genes (*GFAP and Glul)* and two neuronal genes (*Rbfox3 and Pvalb*). As expected, we

173 found a large increase in astroglial gene expression in the bound fragment and a large
174 reduction in neuronal-specific gene expression, suggesting a successful enrichment of
175 the astroglial translatome (Supplemental Figure 3). In order to further characterise
176 astroglial-specific markers by age and sex, we plotted RPKM data for each of the top 20
177 genes expressed only in postnatal neocortical astroglia from both the Cahoy dataset[32],
178 28 genes from the Zhang dataset[38] and 48 genes from the Rowitch dataset that identified
179 layer-specific astroglial cell gene expression (Bayaktar et al. 2020) that were non-
180 overlapping (Supplemental Figures 4, 5 & 6). Interestingly, expression of most astroglia-
181 specific genes from the Zhang and Cahoy datasets (27/48) increases across
182 development, for example *CYP4F14*, a Vitamin E hydoroxylase and *SLC39A12*, a zinc
183 transporter involved in the pathophysiology of schizophrenia[39] both have low expression
184 levels early on and rise to adult levels at P14 (Supplemental Figure 4). Only one astroglial
185 gene decreased in expression over development, *Pla2g3,* a gene involved in oxidative
186 stress that has been linked to Alzheimer's disease[40].

187 Supplemental Figure 5 depicts the 14/48 astroglial genes that show stable
188 expression over development and finally, Supplemental Figure 6 depicts those genes
189 (8/48) that show consistent low expression over the entire developmental period
190 assessed. Interestingly, we did not find any apparent sex differences in these astroglial-
191 specific genes, although a few appear as DEGs at specific time points, for example, the
192 cytokine Il33 is a DEG at P7 (lower in females- see below). Supplemental figure 7 shows
193 astroglial cell gene expression for Layers 2-4 and deep layers 5-6, supplemental figure 8
194 shows upper-layer biased astroglial cell gene expression across development, and
195 supplemental figure supplementary figure 9 shows gene expression for genes identified
196 with the AST2, AST3 subtypes.

197 ***Astroglial cell show age related differences in translatome***

198 Next, we examined the overall sample-to-sample relationship by hierarchical
199 clustering to identify patterns throughout development and across sex. Clustering shows
200 a pattern of organization that is primarily affected by age, with P1, P4 and P7 (early) and
201 P14, P35 and adult mice (late) showing clustered expression patterns that differ from the
202 early time points (Figure 2A). We manually sorted samples by sex and age and although

203 some organization by sex is noted in Figure 2B, this is not as clearly demarcated or as
204 extensive as that observed by age. Indeed, when we collapsed gene expression levels
205 across all time points, only 16 genes were differentially expressed between female and
206 males (Supplementary Data File 2) and a subset of these sex differences in gene
207 expression is for genes are located on the sex chromosomes, suggesting little to no sex
208 differences in neocortical astroglia across all time points overall. However, when we look
209 at sex differences over time, we do note sex differences in developmental patterns. It is
210 clear that there are two major neocortical astroglial phenotypes across age: an early (P1-
211 P7) and late (P14-adult) phenotype. However, male samples show an "intermediate"
212 cluster and begin to show the late or mature astroglial phenotype at P7, whereas females
213 show this phenotype at P14 (Figure 2B).
214
215 To validate the early and late phenotype that we found using TRAPseq, we
216 compared TRAP extracted RNA on six genes differentially expressed between the early
217 and late timepoints, 3 associated with synapse/network maturation (*Gja1, Lynx1, Grin2c*)
218 and three steroid hormone receptors (*Ar, Pgr, Esr1*). Each of these showed a similar
219 pattern of results between TRAPseq and qPCR (Supplemental Figure 10), which is
220 highlighted by the significant positive correlations shown in Supplemental Figure 11. In
221 addition, we further validated the early and late astroglial cell phenotype, by assessing
222 neocortical astroglial cells protein expression using immunohistochemistry of common
223 astroglial markers at similar timepoints. Using the Aldhl1-L10 eGFP+ mice, we quantified
224 expression of the astroglia-specific cytoskeletal filament protein glial acidic fibrillary
225 protein, (GFAP). GFAP expression was not sexually dimorphic across development
226 ($F_{1,41}$=1.259, p=0.268, $H\eta$=0.029), however, there was a main effect of age ($F_{5,41}$=32.271,
227 p<0.001, $H\eta$=0.793) (Figure 3A). The number of GFAP+ cells reached peak levels at P14
228 and remained stable into P35 and adulthood (Figure 3A). Prior to P14, no more than 15%
229 of eGFP+ cells co-expressed GFAP, from P14-onwards approximately 25% of eGFP+
230 cells expressed GFAP, consistent with previous work that has demonstrated that a large
231 proportion of cortical astroglia do not express GFAP under basal conditions (Simard et
232 al., 2018). Next, we quantified the number of cells that expressed vimentin, another

233 intermediate filament protein in astroglial cells, that is generally associated with a stem-
234 like radial sub-type of astroglial cells. A significant interaction of sex by age was found
235 ($F_{5,41}$=3.871, p=0.006, $H\eta$=0.321) (Figure 3B,D), such that females showed significantly
236 more vimentin+ cells compared with males at P7 (t=3.41, p=0.011) and males showed
237 significantly more vimentin+ cells in adulthood (t=3.895, p=0.005) (Figure 3B). Because
238 vimentin expression is associated with astroglial cell neurogenic and stem cell potential
239 and because we observed sex differences in vimentin expression, we quantified the
240 proportion of actively dividing eGFP+ cells across the postnatal period. Using a marker of
241 active s-phase cell division, Ki67, we quantified the percent of Ki67+eGFP+ cells. Ki67
242 was present in less than 2% of the astroglial cell population throughout the postnatal
243 period in both males and females (Figure 3C). There were no significant sex differences
244 across development ($F_{1,41}$=0.862, p=0.358, $H\eta$=0.021), however there was a main effect
245 of age ($F_{5,41}$=26.799, p<0.001, $H\eta$=0.766). Importantly, the findings here that the number
246 of astroglial cells expressing vimentin show sex and age differences, and proportion of
247 astroglia expressing GFAP and Ki67 show distinct early and late expression closely
248 resemble the expression patterns revealed by TRAPseq analysis.
249
250 ***The developmental pattern of the astroglial translatome is sexually dimorphic***
251 To further characterize the *"early"* and *"late"* phenotype observed in the astroglial cell
252 translatome, we examined the number and proportion of up- and downregulated genes
253 in the early versus late developmental phenotypes, both overall and by sex (Figure 4A).
254 The early versus late phenotype in males showed 8983 DEGs whereas the female early
255 versus late phenotype had 9688 DEGs (full list of DEGs in Supplementary Data File 1).
256 Interestingly, the proportion of up- or downregulated genes was similar, with males and
257 females showing 62% and 55% of DEGs in the early versus late phenotype being
258 upregulated, respectively. When we collapsed the DEGs across sex to generate a general
259 early vs late phenotype for astroglial cells, the number of DEGs reaches 12131 with 58%
260 of those genes being upregulated in the late phenotype (Figure 4A). This suggests that
261 the difference in the early and late developmental phenotype is not merely reflective of
262 turning off developmental genes but rather is a combination of downregulating genes

263 associated with early development and turning on genes associated with later neocortical
264 development and basal functioning in early adulthood. Some key DEGs stand out as they
265 have not previously been functionally described in astroglial cells. In particular, *Trim67*,
266 an important and evolutionarily preserved guidance cue for neurite outgrowth[41], is high in
267 early development and, as expected, decreases with age. Additionally, *Ntng1*, codes for
268 Netrin G1, another guidance cue that is paramount to developing neuroblasts, is higher
269 during the "late" developmental phenotype in astroglial cells. Differential *Ntng1*
270 expression appears when examining both the overall and the sex-specific early versus
271 late astroglial cell phenotype. *Ntng1* has been implicated in the etiology of familial
272 schizophrenia[42] and *Ntng1* mRNA is in lower cortical samples from individuals with
273 schizophrenia and autism[43].

274 We compared the proportion of overlap between the female-specific and male-
275 specific DEGs in the early vs late phenotype. Of the 11415 unique DEGs, approximately
276 64% overlap between males and females, however about 21% of total DEGs are specific
277 to females and only about 15% are specific to males (Figure 4B). When we further
278 characterize the sex-specific canonical pathways (CPs) and gene ontology (GO) by gene
279 set over-representation, a proportion of the top five female-specific CPs are related to cell
280 cycle/mitosis, marked by CPs in ribosome function. In comparison, male-specific CPs are
281 related to oxidative phosphorylation and small molecule transport. With respect to GO, a
282 large proportion of the top five female-specific and male-specific GOs are related to
283 intracellular parts and organelles. This suggests that there are distinct developmental
284 patterns in neocortical astroglial cells that emerge between the sexes. To broaden the
285 understanding of sex differences, we identified DEGs of females versus males at each
286 time point (Figure 4C, Supplementary Data File 2). At P1, there are only 20 DEGs,
287 however there are 183 DEGs at P7 and 100 DEGs at P14 (Figure 4C; full list of DEGs in
288 Supplementary Data File 2). Analysis of DEGs at P1 calls one CP related to histone
289 demethylation. When we analyze DEGs between timepoints and sexes, we observe a
290 peak in the number of DEGs when comparing P7 vs 14 in both females and males (Figure
291 4D and Supplementary Data File 3). Within this peak (P7 vs. P14), 1658 DEGs are
292 identified in males and 3685 DEGs are identified females. These sex differences between

293 P7-P14 are particularly striking given that these are the developmental time points, where
294 sex hormones are largely dormant. This suggests that these sex differences in astroglial
295 gene expression are part of a developmental program induced by perinatal exposure to
296 hormones involved in sexual differentiation and/or directly induced by sex-linked
297 chromosomes. Remarkably 39% of DEGs at P7 and 79% of DEGs at P14 are
298 downregulated in females. Within these downregulated genes are typical markers of cell
299 activity, the immediate early genes *Fos* and *Arc*, suggesting decreased basal activity in
300 female astroglial cells at these timepoints (Supplementary Data File 3, Tab a). Analysis
301 of DEGs at P7 show that three of the top five CPs are related to synapse development
302 and transmission while the remaining two are related to intracellular signalling pathways.
303 Similar analysis of DEGs at P14 show that the majority of the top five CPs are related to
304 cell cycle. In addition, the top five GO terms from DEGs at P7 are related to myelination
305 and synaptic components and at P14, the top five GO terms are related to cell cycle.
306 A more complete view of sex differences is captured by differential network
307 dynamics. We used co-expression network analysis (see Online Methods), to infer,
308 separately a co-expression network in females and males throughout development, and
309 identified 10 "female" (F) and 12 "male" (M) co-expression modules, plus one unassigned
310 gene module, grey (Supplementary Data File 4 & Supplementary Data File 5, Tab1). In
311 females, the F3, F6, F7 and F9 modules are enriched in genes upregulated in late vs.
312 early, and the F1, F2, F4 and F10 modules are enriched in genes downregulated in late
313 vs. early (see Supplementary Data File 4,Tab4). The F3, F6 and F9 (upregulated)
314 modules are enriched in astroglial genes. The F2 and F4 modules (downregulated) are
315 enriched in cell cycle terms, and the F10 module (downregulated) is enriched in genes
316 involved in proteasome activity and cell cycle. In the males' network, the M2, M3, M4, M8
317 and M12 modules are enriched in genes upregulated in late vs. early, and the M1, M7
318 and M10 modules are enriched in genes downregulated in late vs. early in males (see
319 Supplementary Data File 5, Tab 4). Similar to what was observed in the female network,
320 some of the modules enriched in upregulated genes in the late vs. early phenotype in
321 males (M2, M3, M6 and M8), are enriched in astrocyte genes. It is likely that, in both
322 networks, the astrocyte signature for the modules enriched in upregulated genes reflects

323 a shift in a mature astroglial phenotype during development. Finally, the M10 module
324 (downregulated) is enriched in cell cycle terms, and the M1 module (downregulated) is
325 enriched in genes involved in mRNA processing. The cell cycle signature for some of the
326 downregulated modules likely reflects a reduction of proliferative potential of the cells over
327 time, as would be expected over development.

328 We conducted an eigengene analysis of the network modules to evaluate how
329 modules changed over development. Overall, we found consistent results across males
330 and females whereby modules enriched with astroglial genes were increased over
331 development, modules enriched with genes involved in cell cycle regulation were
332 downregulated over development, modules involved in translation (ribosomes) were also
333 downregulated and finally modules enriched in genes related to mitochondria and
334 mitochondrial function were increased with age, further lending support to the "early" and
335 "late" astroglial cell phenotypes (Supplementary Data File 5, Tab 4 and Figure 5 A-C).

336 A closer look at the temporal dynamics highlights some interesting features, with
337 the female network characterized, mostly, by monotonic, sigmoid like temporal profiles,
338 and the male network characterized by a larger variety of patterns (subset shown in Figure
339 5 A-C). In females, the sigmoid profiles are either decreasing with age (F1, F2, F4 and
340 F10) or increasing with age (F3 and F9). We also find two modules (F6 and F7),
341 increasing with age, with a possible peak at P7 and P14, respectively. In the sigmoid
342 profiles, we also identified a 'slow' subgroup (F1, F2 and F9), characterized by a slow
343 change between P1 and P7 and more activity around P14; and a 'fast' subgroup (F3, F4,
344 F5, F7 and F10), characterized by a fast change around P7 and lower activity from P14
345 onward. The temporal dynamic pattern analysis is consistent with the "early" and "late"
346 hierarchical clustering. Unlike the female network, most of the modules in the male
347 network show a relatively faster temporal dynamics at P1 to P4-P7. Noticeable are also
348 the pronounced early peaks in the M5 and M6 modules, the late peaks in the M4, M8 and
349 M12 modules and a pronounced deep at P7 in the M10 module. Functional analysis
350 shows that the 'early peaks modules', M5 and M6, are enriched in neurotransmitter
351 secretion and synaptic transmission terms, respectively; the 'late peaks' modules, M4,
352 M8 and M12, are enriched in transmembrane transport, signaling receptor

353 activity/astrocyte, and transmembrane transport terms, respectively. The M10 module is
354 enriched in mRNA processing, and the M1 in neuron terms.
355 We tested the modules for enrichment in Estrogen and Testosterone related gene
356 sets (i.e. ESR1 and ESR2 gene targets and genes/proteins interacting with the
357 chemical Testosterone (Rouillard et al., 2016) and found significant overlap between the
358 M2 module in males with the ESR1 targets. The male M2 module expression increases
359 rapidly, from P1 to P14, where it levels off. This may be consistent with the active process
360 of masculinization of the brain early in development. No significant overlap is found with
361 any of the modules in the female set.
362
363 ***Network dynamics highlight differential astrocyte subtype differentiation***
364 We tested the male and female modules for enrichment in gene marker for
365 astrocyte sub-types (Bayraktar et al., 2020; Nature Neuroscience; Batiuk et al., 2020;
366 Nature Communications) to investigate sexual dimorphism in astrocyte subtype
367 differentiation, and describe them following the developmental timeline (see
368 Supplementary Data File 4, and Supplementary Data File 5, Tab5).
369 The AST4 (neural stem or progenitor cells) markers overlap with modules F2, F6
370 and F10 in females, and M1, M8 and M11 in males. The overlap with modules decreasing
371 with time is expected and in line with the stem cell/progenitor phenotype of AST4, while
372 the overlap with F6 (females) and M8 (males) is more surprising, given that both modules
373 first decrease, then increase from P7 (see Figure 5B). Interestingly, vimentin expression
374 is one of the major markers of the AST4 subtype (Batiuk et al., 2020; Nature
375 Communications) (in Supplementary Data File 2), therefore our observation of sex
376 differences in vimentin expression over time (Figure 3B) is consistent with sexual
377 dimorphism in these particular network dynamics.
378 The AST5 (intermediate progenitors) markers overlap with F3 and F9 in females
379 and M1, M2 and M6 in males (see Figure 5C). All modules show increased expression
380 over time at a faster rate than modules overlapping with the mature astrocytes, and
381 differently in males than in females. Interestingly, in males, we find overlap with module,
382 M1, a module decreasing over time, and lack of overlap with a similar module in females

383 (see Figure 5C). Top scoring terms for this module are mRNA processing, Spliceosome
384 and Proteasome. Down-regulation of this module could be associated with cell cycle and
385 the associated dismantling and ciliogenesis of astroglial cilia (Sterpka and Chen, 2018).
386 Alternatively, the proteasome gene down-regulation could also be consistent with the
387 GFAP increase over time (Middeldorp et al., 2009). The faster temporal dynamics and
388 the male specific module point to sexual dimorphisms in astroglial differentiation
389 dynamics that become explicit at the intermediate progenitor stage; these warrant further
390 investigation in future studies.

391 The AST1, AST2 and AST3 (mature astrocytes) markers overlap with modules
392 showing increasing expression with time both in females (F9 and F3) and in males (M2,
393 M3 and M12). Notably, the F9 module in females (AST1, AST2) has a slower rise than
394 F3 (AST2, AST3), suggesting a delay in AST3 with respect to AST1 (see Figure 5A). In
395 males, M2 is enriched in all the mature cell types, probably capturing common underlying
396 processes; the M12 (AST1, AST2) module starts increasing late, at P14, M3 has a slower
397 increase with respect to M2, again suggesting a delay in AST3 differentiation with respect
398 to AST1 and AST2. The overlap with modules increasing expression in time is consistent
399 with the mature phenotype of these astroglial classes. Overall, some female modules
400 show little change between P1 and P4, and a steeper increase from P4 to P7, while male
401 modules tend to change from P1, suggesting a delay in females. Also, we find two shared
402 modules in males, across two transitions, M1 in AST4 to AST5, and, M2, in AST5 to
403 AST1/AST2/AST3; conversely, females do not have any shared modules in the first
404 transition, AST4 to AST5, and have two shared modules, F3 and F9, both in the second
405 transition AST5 to AST1/AST2/AST3.

406

407 **Differential Transcriptional Regulation Dynamics Drives Sexually Dimorphic**
408 **Astrocyte Differentiation Programs**

409 The different developmental trajectories and the faster temporal dynamics in
410 males supports the idea of differential regulation of astrocytic differentiation ?between
411 males and females, already present at P1. We then investigated the regulation of network
412 modules to identify determinants of network dynamics and subtype differentiation. We

413 first identified a number of putative transcription factors regulating the male and female
414 network modules and found an average of 320 and 340 significant TFs per module,
415 respectively, for a total of 856 and 858 TFs (see Methods), with 2 male-specific (HELT,
416 KAT7) and 4 female-specific (CARF, CPEB1, MTF1, PHF1 TFs. Interestingly, HELT and
417 CPEB1 target AST4 genes markers involved in different processes (HELT: neural crest
418 differentiation, cell fate specification; CPEB1: cell cycle related; cell projection;
419 cytoskeleton) (see Table GF4 and GF5 Tab6).

420 We then used the expression of TFs target genes as a reporter of activity, similarly
421 to the Viper algorithm (Alvarez et al., 2016), and estimated TF differential activity between
422 females and males at each time point, and between time points, using the camera
423 algorithm (Wu and Smyth, 2012) (see Methods).

424 We first identified the subsets of differentially active TFs (DATFs) between P1 and
425 P4 in males and females, as putative determinants of early transcriptional dynamics,
426 resulting, respectively, in a set of 839 and 510 DATFs, respectively. Within this subset,
427 we identified DATFs at P1 between males and females, as putative TFs driving the
428 difference in early transcriptional dynamics, resulting, respectively, in a set of 775 and
429 119 DATFs, suggesting a stronger activity in transcriptional regulation in males vs
430 females. Next, we focused on the subset of DATFs targeting gene markers of individual
431 astrocyte sub-types, to focus on cell-type specific differential regulation. We found 551
432 DATFs in males and 33 in females, with targets co-expressed in the modules M1 (57),
433 M11 (494) and F2 (24), F10 (9), and enriched marker genes for AST4. At P1, the already
434 consistent number of differentially active TFs might reflect the differential priming by
435 testosterone and/or aromatization of estradiol in males of astrocyte progenitor cells, which
436 would reach peak levels at this time. Interestingly, ESR1 is a DATFs controlling targets in
437 M11, suggesting that some of the sex differences in the developmental trajectories of
438 cortical astroglia, may be directly initiated by the perinatal exposure to estradiol critical to
439 male sexual differentiation.

440 We then aggregated the TF-target genes and built a regulome (i.e. a regulatory
441 network represented as a directed graph) for the males (13536 genes and 404928 edges)
442 and females (13756 genes and 449097edges) using known regulatory relationships, and

443 identified the putative TFs, potentially upstream of the other TFs/genes, i.e. the source
444 nodes of the graph (see Methods). The source nodes are the nodes in a directed graph,
445 with a non-zero out-degree and a zero in-degree. We found ESR1, ZFP3, MZF1, PRRX1,
446 SOX7, MSX2, ZGPAT, TCF24, and MYRFL in the male network and BARX2, FOXR2,
447 and MYRFL in the female network. Interestingly, while ESR1 is present in both, it is a
448 source node only in the male network, supporting a central role of ESR1 in AST
449 differentiation in males and of network rewiring early in masculinization.

450 Early masculinization of the brain occurs largely as a result of a perinatal surge in
451 testosterone that is aromatised into estradiol in the brain of males, therefore we further
452 examined P1 as a critical time point in setting up differential developmental patterns in
453 the astroglia of males and females. Extensive work from the McCarthy laboratory has
454 demonstrated that prostaglandins, and specifically, glial release of cyclooxengase 2
455 (COX-2) is a key regulator of estrogen-mediated architectural sex differences in the
456 hypothalamus and the amygdala[44,45]. The gene for COX2, *Ptgs2*, is a sex-specific DEG
457 in our data set, in the overall females versus males analysis, in the early female versus
458 male phenotype, and at P1 female versus male comparison (Supplementary Data File 1
459 & Supplementary Data File 2) Furthermore, Cox2 is listed as an ESR1 target in our
460 dataset and it is well- known to be downstream of ESR1 signalling (Stossi et al., 2004).
461 To validate COX2 expression over development, we counted the number of cortical
462 COX2+ cells in astroglia (co-localised with eGFP) and saw a similar pattern of expression
463 to that observed in our TRAPseq, with a significant sex difference in astroglial Cox2
464 protein expression at P1 ($F_{1,41}$=12.517 p=0.017, $H\eta$=0.715)(Figure 6A). COX2-mediated
465 masculinization of the hypothalamus occurs in response to estradiol, which is aromatised
466 from the surge in testosterone in males that occurs perinatally in rodents (Figure 6B). This
467 perinatal surge in testosterone has been linked to sexual differentiation of the
468 hypothalamus, amygdala, and mediates sexually dimorphic juvenile and adult
469 behaviours[46-48]. To validate our findings and to test if astroglial COX2 protein levels are
470 similarly regulated by estrogen in the cortex, we compared vehicle injected males and
471 females with females that were masculinized by injecting estradiol benzoate at P0 and
472 then sacrificed all groups 36 hours later. The overall one-way ANOVA showed a trend for

473 significance ($F_{3,20}$=2.781, p=0.068, $H\eta$=0.294), however because our previous
474 experiment showed a difference between males and females, we conducted a planned
475 comparison of these groups. Females at P1 show fewer COX2+ cells in the frontal cortex
476 compared to males ($F_{1,9}$=7.827, p=0.021, $H\eta$=0.465) and females exposed to estrogen
477 ($F_{1,9}$=5.759, p=0.04, $H\eta$=0.390) (Figure 6C). This suggests that estrogen exposure at
478 P0 is sufficient to masculinize COX2 expression the cortex.
479
480 **(Sex differences in) Astrocyte differentiation and relevance to disorders**
481 We investigated the relevance of the male and female co-expression network to human
482 disease, by testing the network modules for overlap with disease ontologies (DOs) (see
483 Methods). We focused on the subset of the modules in overlap with astrocyte subtype
484 markers, and report only results for brain-specific disorders (see Supplementary Data File
485 4 & Supplementary Data File 5, Tab7). In females, top scoring DO terms are intellectual
486 disability and mental deficiency (Module F2); intellectual disability, bipolar disorder,
487 epilepsy, schizophrenia, cognitive delay, autistic disorder, Alzheimer's disease (Module
488 F3); Unverricht-Lundborg syndrome, lysosomal storage diseases, amyloidosis,
489 progressive myoclonic epilepsies (Module F6); epilepsy seizures, Alzheimer's disease,
490 schizophrenia, intellectual disability, major depressive disorder, neurodegenerative
491 disorders, autistic disorder, Parkinson's disease (Module F9). In males, top scoring DO
492 terms are intellectual disability (Module M1); mitochondrial diseases, Alzheimer's
493 disease, neurodegenerative disorders, epileptic encephalopathy, seizures, bipolar
494 disorder, epilepsy, schizophrenia, autistic disorder, Parkinson's disease (Module M2);
495 peripheral neuropathy (Module M3); mitochondrial diseases, Leigh disease (Module M6);
496 intellectual disability (Module M8); microcephaly, ciliopathies, intellectual disability
497 (Module M11); epilepsy, bipolar disorder, mental depression, unipolar depression,
498 depressive disorder, Alzheimer's disease, schizophrenia, Intellectual disability, autistic
499 disorder (Module M12). Notably, many of the diseases are in overlap between males and
500 females, and there does not appear to be disease specificity per se as a wide variety of
501 neurological, psychiatric, and developmental disorders are called. Importantly, however,
502 each of these diseases have been linked to astroglial dysfunction either primarily or in a

503 reactive capacity and therefore the wide variety of diseases called likely speaks to the
504 general involvement of astroglia in all neural processes (Molofsky et al., 2012). Modules
505 associated to differentiated astrocyte subtypes, i.e. increasing with age, are enriched in
506 neurodegenerative disorders terms. Interestingly, these same modules also show
507 enrichment in autism-associated genes, and only modules F9 and M2 show enrichment
508 in Parkinson's disease genes, unlike Alzheimer's and schizophrenia. Perhaps reflecting
509 regional involvement in disease pathology, with Parkinson's origins to mid-brain-striatal
510 functions rather than cortical origins. Module F6, associated with astrocyte progenitor
511 cells, is enriched in epilepsy related genes including a number of GABA transporters and
512 GABA receptor subunits (*gabra3, gabrg2, gabrb2, slc6a1*), unlike its M8 counterpart.
513 Interestingly, both astroglial cells and GABA subunits are central to epilepsy pathology
514 (Coltour and Steinhäuser, 2015; Fritschy, 2009), and sex differences in gaba subunits
515 have been linked to sex differences in epilepsy (Li et al., 2007) however, whether
516 astroglial expression of these subunits is related to developmental sex differences in
517 epilepsy susceptibility is unknown. Finally, the "early peak" module M6 associated with
518 intermediate progenitor cells, is enriched in mitochondrial diseases terms. This male-
519 specific expression is consistent with mitochondrial diseases having a higher incidence
520 in males, thought to be due to uniparental or maternal inheritance (Beekman et al., 2014).
521
522
523
524

525 Discussion

526 In the current study, we generated a translatome database of cortical astroglial
527 cells across development in both male and female mice. We show two clear astroglial
528 phenotypes across development, an early (before P14) and late (after P14) phenotype.
529 These early and late gene expression profiles reflect astroglia associated with early
530 developmental functions related to gliogenesis and synaptogenesis and astroglia
531 associated with functions involved in maturation, synapse elimination and maintaining a
532 stable, homeostatic environment in adulthood (Figure 7D).

533 Surprisingly, cortical astroglial cells showed very little sexual dimorphism in either
534 morphology or gene expression particularly in adulthood when very few DEGs were not
535 sex-chromosome associated genes. Importantly, to assess basal differences between
536 males and females in a conservative way, we chose to examine females during the
537 metestrus phase, when ovarian hormones are at their lowest and therefore more similar
538 to levels observed in males. As such, it is likely that greater sex differences in the
539 astroglial translatome would be observed during other estrous cycle phases, such as in
540 proestrus, when estrogen peaks. Indeed, we have previously demonstrated changes in
541 cortical astroglial expression of GFAP and fibroblast growth factor 2 (FGF2), an astroglial
542 mitogen and growth factor across the estrous cycle[49], and a number of studies have
543 shown functional, morphological and protein expression changes in astroglia in response
544 to sex hormones (Verkhratsky and Nedergaard, 2018; Azcoitia et al., 2010) Together
545 these results would suggest that astroglial cells show phenotypic changes in response to
546 ovarian hormones (or activational effects of hormones), but at least in the neocortex,
547 astroglia do not show basal sexual dimorphism (organizational effects of hormones).

548 Interestingly, the sex differences in DEGs observed at P7,and P14, were not
549 related to sex-specific canonical pathways or functions per se, but rather, were related to
550 general developmental phenomena such as cell cycle, and neuronal, dendritic and
551 synaptic development, suggesting that astroglia modulate neuronal networks in a sexually
552 dimorphic way. This could, in turn, potentially lead to the formation of sexually dimorphic
553 neuronal networks, and presumably, sexually dimorphic behavioural expression later in
554 life. Given the critical role of the neocortex in psychiatric disease and complex human

555 behaviours[50], one might imagine that changes in neuronal network development may be
556 induced by estrogen-modulated changes in astroglia. In addition, these may be
557 particularly susceptible to developmental perturbations that modulate hormone
558 expression levels including exposure to stress hormones and environmental endocrine
559 disruptors. Moreover, because hormone levels vary between individuals under normal
560 conditions, this allows for a potential range of sexual differentiation of cortical networks,
561 which would mirror behavioural sex differences observed across species, that are
562 typically expressed on a continuum.

563 In contrast to the sex differences in gene expression seen in P7-P35, we see few
564 DEGs between astroglia in male and female mice in the early postnatal period and in
565 adulthood. This, in addition to the sex differences in CP of early versus late astroglial
566 phenotype and the apparent early peak of some networks in male mice, suggests that
567 cortical astroglial cells employ different developmental strategies or timing in
568 developmental trajectories to reach a similar adult phenotype, with males accelerating
569 faster than females in early development. The idea that distinct developmental trajectories
570 between the sexes might lead to similar functional results is similar to the concept of
571 compensation put forward by Woolley[51], which was based on findings of estradiol
572 potentiating glutamatergic synapses, albeit on a much more general level. Earlier
573 DeVries[52] postulated that sex differences in gene expression patterns over development
574 may actually prevent sex differences in specific regions or ensure that neuronal systems
575 develop and are functional in the presence of cues such as sex hormones that are crucial
576 for stimulating sex differences in target regions. It is possible that the sex differences in
577 gene expression profiles between astroglia ensure that these systems develop "equally"
578 in both sexes to achieve similar functionality in adulthood in the presence of sex
579 chromosomes and hormones that are necessary to differentiate regions critical to sexually
580 dimorphic behaviours, such as the hypothalamus.

581 The question remains as to what induces sex differences in cortical astroglia gene
582 expression patterns over development. Three potential scenarios emerge: 1) sex
583 chromosome-linked genes directly induce changes in gene expression patterns in
584 astroglia. 2) The perinatal testosterone surge initiates cascades of gene expression

585 patterns in astroglia that modulate cell maturation and network development. 3) Astroglial
586 cells have a similar start and end point in our dataset and it is possible that sex differences
587 in astroglia gene expression represents an active process to compensate for sex
588 differences in developing neuronal imputs to the cortex that arise from dramatic changes
589 in neuronal number, arbours, and synapses on neurons that project from the
590 hypothalamus to the neocortex Importantly, these scenarios need not be mutually
591 exclusive and may be active in parallel systems.

592 *Scenario 1. Kdm5d* appears as one of the few DEGs between females and males
593 at P1 in our dataset, female expression levels are lower than males. *Kdm5d* is a Y-linked
594 gene that encodes for demethylation enzymes and is required and sufficient to induce
595 sexual differentiation of gene expression[53]. Indeed, changes in gene methylation may
596 have profound effects that persist throughout time and cascades of gene expression may
597 or may not be initiated, altering the responsiveness of the cell, and thus the network as a
598 whole. Moreover, even in the absence of the testes determining *Sry* gene, the Y-
599 chromosome has been shown to exert differential effects on developing peripheral and
600 nervous tissue (reviewed in[54]), lending support to the idea that sex chromosome linked
601 genes induce later sex differences in astroglia across development.

602 *Scenario 2.* Similarly, our results suggest that the perinatal testosterone surge, and
603 consequentially, estrogen, is involved in the induction of developmental sex differences
604 in astroglia. Our weighted network analysis shows enrichment of genes in several
605 modules associated with responses to sex hormones. We show sex differences in the
606 prostaglandin system (including Cox2) and that neonatal estrogen administration induces
607 changes in cortical COX2 expression. Similar changes in astroglia have been
608 demonstrated in the hypothalamus and are sufficient to produce observable sex
609 differences in neuronal networks and associated behaviour[13]. Thus, the endogenous
610 expression of estrogen early in development may facilitate a cascade of cellular
611 maturation that in-turn will alter subsequent genetic programs. As such, the neuronal
612 network will facilitate different programs as a result of the staggered pattern of maturation
613 and communication.

614 Finally, *scenario 3* suggests that sex differences in the hypothalamus are
615 necessary for a functional behavioural outcome that is overt and essential for sexual
616 reproduction, first suggested by de Vries[52]. However, there are few overt measures that
617 can be linked to cortical functioning that exhibit similar sexual dimorphisms, although sex
618 differences in risk and resilience for psychiatric disease associated with cortical
619 functioning are well-supported. For example, schizophrenia and ASD are more prominent
620 in the male population[8] and both show changes in developmental pathophysiology that
621 occur both during the prenatal and postnatal periods[55,56]. There may be a relationship
622 between astroglial neurogenic potential and the terminal phases of neuronal migration
623 and construction and maturation of functional cortical networks that buffers females
624 against developmental anomalies which, if left unchecked, may lead to schizophrenia or
625 ASD morbidity.
626 In-line with this hypothesis, there are a number of models where estrogen
627 treatment improves recovery or where females are protected in developmental injury
628 models. Chronic postnatal hypoxia in rodents is used as a model of premature birth and
629 induces loss of brain volume, particularly in the cortex and hippocampus, and leads to
630 motor and cognitive impairments later in life[57,58]. The loss of cortical volume in the hypoxic
631 model is less pronounced in females[57] and interestingly, estradiol treatment at the time of
632 the injury improves white matter damage recovery[59]. It is also known that chronic
633 postnatal hypoxia increases astroglial stem cell capacity[25,60]. This process may be
634 enhanced in females allowing augmented recovery from the aversive effects of hypoxia,
635 but may also speak to the nature of enhanced early postnatal plasticity in females
636 compared to males. It is possible that females experience an enhanced or shifted
637 neurogenic period early postnatally, when we have observed an increase in vimentin+
638 astroglia, that may translate to increased neurogenic potential of astroglial cells in the
639 cortex. Similarly, while overt network or cellular sex differences may not modulate sex
640 differences in risk for psychiatric disease, sex differences in developmental programs may
641 leave one sex more vulnerable to perturbations during that time. Future studies will be
642 needed to determine the functional significance of sex differences in developmental
643 programs. Nevertheless, our data show a clear developmental pattern in cortical astroglia

644 that differs between males and females, while no apparent basal sex differences in
645 astroglia exist.
646
647

648 Online Methods

649 *Animals*

650 54 male and female C57/Bl6-AldHl1-L10-GFP transgenic mice generated from our
651 breeding colony maintained at the Carleton University animal facility within the University
652 of Ottawa. Mice were genotyped as in (Simard et al., 2018) and sex was determined by
653 the presence or absence of tissues in the urogenital tract and confirmed by genotyping
654 for the *Zfy* gene. All animals were group-housed until sacrifice in standard (27cm x 21cm
655 x 14cm), fully transparent polypropylene cages with chew block, bedding, house and *ad*
656 *libitum* access to standard lab chow (2014 Teklad Global 14% protein®) and water.
657 Animals were raised in the standard environment with no outside manipulation except for
658 standard care and to monitor estrous cycle stage (when applicable). The mice were
659 maintained on a 12-hour light/dark cycle in a temperature controlled (21 degrees) facility.
660 All animal use procedures have been approved by the Carleton University Committee for
661 Animal Care, according to the guidelines set by the Canadian Council for the Use and
662 Care of Animals in Research. Mice were overdosed and perfused for
663 immunohistochemistry or rapidly decapitated for TRAPseq processing each on postnatal
664 day 1* (P1) (36 hours postnatal), P4, P7, P14, P35 and adulthood (defined as 7-9 weeks
665 of age) at the same time of day. Developmental time points and subject numbers are
666 summarized in Supplementary Figure 1.

667 Organizational hormones study- 5 pregnant dams were ordered from Charles
668 River and arrived at the Carleton University animal facility at the University of Ottawa at
669 gestational day 15/16 and given 3 days to acclimatize to the environment. Dams were
670 monitored intermittently overnight starting on gestational day 19 using red light. 31 male
671 and female pups were randomly assigned to control or treatment groups approximately 1
672 hour following birth and sacrificed 35 hours later. The majority of groups in all experiments
673 were formed with subjects from 3-5 separate litters to control for litter effects.

674 *Estrous Cycle Monitoring*

675 All adult group female animals were monitored daily after P35 to identify stage of
676 estrous cycle using a saline lubricated swab inserted into the opening of the vagina to
677 collect cells from the vaginal wall. Samples were smeared on a glass microscope slide

678 and examined under a 10x objective using a light microscope (VistaVision™). To
679 understand basal organizational sex differences in astroglia, we used female mice in the
680 phase of the estrous cycle with the lowest circulating ovarian hormones that has the least
681 effect on cortical astroglial morphology and protein expression: metestrus[61]. After the
682 stage of estrous cycle (Metestrus, Diestrus, Proestrus and Estrus) had been established
683 for at least two full cycles, females were sacrificed during the light cycle of the metestrus
684 stage.

685 *Organizational hormones-injections*

686 Estradiol benzoate (Chem Cruze, sc-205314) was dissolved in peanut oil
687 (0.8g/mL) as per Hisasue et al., 2010 to allow for an injection of 20µg in a 25µL injection
688 volume. Letrozole (Sigma-Aldrich, LG545-10MG) was dissolved in 0.3% hydroxypropyl
689 cellulose PBS (Aldrich, 435007-5G) as per[62], to allow for an injection of 250mg/kg in a
690 25µL injection volume, sufficient to block all testosterone conversion based on average
691 pup weight of 5g. Estradiol benzoate and letrozole solutions were prepared using glass
692 materials and stored in a glass amber bottle to prevent absorption and disruption from
693 plastics or ultraviolet exposure.

694 *Animal Sacrifice*

695 *Rapid Decapitation for immunohistochemistry and qPCR-* Animals in the P1
696 immunohistochemical group were rapidly decapitated and brains immediately placed in a
697 4% paraformaldehyde (Fisher Scientific) (PFA) solution at 4 ºC for 24h after which the
698 brains were switched to 30% sucrose at 4 ºC for 24h. Following this period, brains were
699 flash frozen until slicing. For the organizational hormone experiment, pups underwent
700 rapid decapitation 36h following treatment. Brains were harvested and split along the
701 central fissure. One hemisphere was flash frozen at -80°C for analysis in qPCR and the
702 other hemisphere was fixed as above.

703 *Cardiac Perfusion for Immunohistochemical Analysis-* All mice were sacrificed for
704 tissue collection at the same time of day during the light cycle. All mice in the
705 immunohistochemical group underwent cardiac perfusion aside from those in group P1
706 (see above). Animals in P4, P7, P14, P35 and adult groups were given an overdose of
707 44mg/kg sodium pentobarbital (CDMV Canada), followed by intra-cardiac perfusion upon
708 all spinal reflex cessation. Animals from the P4 and P7 groups underwent manual cardiac
709 perfusion with 1mL of saline solution before receiving 1mL of 4% PFA via syringe. Mice
710 in the P14, P35, and adult groups blood were flushed using 10mL of saline through the
711 left atrium followed by 20mL of 4% PFA to fix the tissue. Brains were extracted and placed
712 into vials containing 4% PFA and stored at 4 ºC. Following a 24h period, brains were
713 transferred to a 30% sucrose in PBS (Fisher Scientific) solution and placed at 4 ºC.

714 *Tissue sectioning*

715 Following sucrose treatment, all brains were then flash frozen at -80 ºC until
716 sectioning on a Leica (Leica™ CM1900) cryostat (30µm thick). 15 sets of sagittal sister
717 sections were adhered to electrostatic slides (Fisher Scientific™) in rotating order, each
718 slide therefore contained a full representation of the brain for stereological analysis as per
719 previous studies[60,63].

720 *Immunohistochemistry*

721 All immunohistochemical processes took place at room temperature (~21 ºC) as
722 per our previous studies[25,60,64]. One representative slide was taken from every subject
723 and all subjects were processed simultaneously. Brain tissue from all groups were

724 prepared for immunohistochemistry using a 10% horse serum (Gibco™) PBS-T (0.3%
725 TritonX (Fisher Scientific)) pre-block solution for 1 hour before being incubated with the
726 respective primary antibody solution (see Supplementary Figure 1). Primary antibodies
727 were diluted in 10% horse serum PBS-T (0.3% TritonX). Following approximately twenty-
728 four hours of primary antibody incubation, slices were washed in a 1x PBS solution 3
729 times to remove unbound antibodies before being incubated with the species-appropriate
730 fluorescein conjugated secondary antibody for visualization. Secondary antibodies were
731 diluted in 10% horse serum PBS-T (0.3% TritonX) and incubated for 2 hours before slides
732 were submerged in a 1x PBS wash 3 times to remove unbound antibodies. Slides were
733 then coated with a nuclear stain, DAPI with hard setting mounting medium (VectorLabs),
734 to fix glass cover slips and allowed to set before analysis. See Supplementary Figure 1
735 for antibodies and dilutions used.

736 *Stereological Analysis*

737 Unbiased estimates of cell numbers were obtained through use of Zeiss
738 AxioImager M2 with ApoTome motorized fluorescent microscope (Carl Zeiss, Thornwood,
739 NY, USA) in conjunction with a motorized stage and a computer running on Windows 7
740 using the program StereoInvestigator™ (MicroBrightfield, Colchester, VT, USA). Serial
741 sagittal sections of the right hemisphere obtained through cryosectioning at 30µm on 15
742 sister sections were used for stereological analysis. Contours encompassing the whole
743 right hemisphere neocortex on each section were drawn as boundaries in
744 StereoInvestigator™. Cells were counted for expression of individual and/or co-
745 expressed proteins using the optical fractionator probe at 40x. Sampling grids were
746 optimized for cortical contours to include at minimum 3 sampling sites per contour to allow
747 for a systematic and unbiased method to estimate cell density and cell quantification for
748 right hemisphere of the cortex regardless of cell shape, size, orientation, spatial
749 distribution, or post-mortem brain shrinkage[65]. Sampling boxes are randomly placed by
750 StereoInvestigator™ within the sampling frame measuring 150µm x 150µm x 30µm with
751 3 of 6 exclusion borders. Total number of cells per count are reported via
752 StereoInvestigator™ output. For analysis of astroglial morphology, StereoInvestigator™
753 (MBF, Vermont ™) software on a Zeiss Observer with Apotome (Zeiss™) was employed.

754 We identified and distinguished between radial and non-radial astroglial cells, counting
755 these using unbiased sampling via the StereoInvestigator (MBF, Vermont ™) at 40x.
756 Representative confocal mosaic images used for photomicrographs were taken using
757 ZEN software (Zeiss™) with the Airyscan 800 microscope (Zeiss™).

758 *TRAPseq*

759 Translating ribosome affinity purification (TRAP)-sequencing was performed as
760 per[66]. Briefly, eGFP-positive animals were rapidly decapitated and the brains removed
761 and placed into a 1000x activated cyclohexamide (CHX) (100µg/ml, Sigma, dissolved in
762 methanol, American Bioanalytical) dissection buffer at which point the cortex, removing
763 any remaining white matter was dissected and flash-frozen in CHX dissection buffer at -
764 80°C. When appropriate, brains were thawed on ice in homogenization buffer containing
765 protease inhibitors, 1000x activated CHX, and RNAse inhibitors. Tissue samples were
766 mechanically homogenized and then incubated on a rotisserie with anti-GFP (HtzGFP_04
767 (clone19F7) and HtzGFP_02 (clone 19C8): Memorial Sloan-Kettering Monoclonal
768 Antibody Facility) coated biotinylated magnetic beads (Streptavidin MyOne T1
769 Dynabeads; Invitrogen # 65601) coated with Protein L (Fisher # PI-29997) at 4 ºC
770 overnight. Following incubation with magnetic beads, the samples were collected on a
771 magnet (DynaMag-2; Invitrogen #123-21D) and the unbound fragment was collected and
772 frozen at -80 ºC. Bound mRNA fragments washed in polysome buffer underwent RNA
773 extraction with DNAse treatment using Absolutely RNA Nanoprep Kit (Stratagene
774 #400753).

775 RNA samples were sent to the Yale K.E.C.K facility for sample QC as per Simard
776 et al. 2018: RNA quality was determined using a nanodrop and RNA integrity was
777 determined by running an Agilent Bioanalyzer gel (RINs >8). mRNA was purified from
778 approximately 500ng of total RNA with oligo-dT beads and sheared by incubation at 94C.
779 Following first-strand synthesis with random primers, second strand synthesis was
780 performed with dUTP for generating strand-specific sequencing libraries. The cDNA
781 library was then end-repaired and A-tailed, adapters were ligated and second-strand
782 digestion was performed by Uricil-DNA-Glycosylase. Indexed libraries that met
783 appropriate cut-offs for both were quantified by qRT-PCR using a commercially available

784 kit: Kapa Library Quant Kit (Illumina) (KAPA Biosystems # KK4854-07960298001) and
785 insert size distribution was determined with the LabChip GX or Agilent Bioanalyzer. Only
786 samples with a yield of ≥0.5 ng/ul were used for sequencing.

787 Sample concentrations were normalized to 10 nM and loaded onto Illumina Rapid
788 or High-output flow cells at a concentration that yields 130-250 million passing filter
789 clusters per lane. Samples were sequenced using 75bp paired-end sequencing on an
790 Illumina HiSeq 2500 according to Illumina protocols. The 6bp index was read during an
791 additional sequencing read that automatically follows the completion of read 1. Data
792 generated during sequencing runs were simultaneously transferred to the YCGA high-
793 performance computing cluster. A positive control (prepared bacteriophage Phi X library)
794 provided by Illumina is spiked into every lane at a concentration of 0.3% to monitor
795 sequencing quality in real time.

796 *Quantitative Real-Time PCR*

797 To validate the enrichment of astroglial cell genes in our bound,
798 immunoprecipitated fragment, the astroglial specific genes GFAP and Glul expression
799 levels were compared between input and TRAP-immunoprecipitated fragments. In
800 addition, we evaluated RbFox3 and Pvalb gene expression assays to validate a
801 concurrent decrease in neuronal gene expression. 20ng of RNA (concentration
802 determined using NanoDrop (Thermofisher Scientific)) was used to produce cDNA using
803 SuperScript IV First Strand Sythesis System (ThermoFisher Scientific). Best-coverage
804 TAQMAN assays (Life Technologies) were run as per manufacturer's instructions and
805 analyzed using the Applied Biosystems 7500 Real-Time PCR system and software.

806 To validate the TRAP-seq results we used RNA from all bound (*n*=55),
807 immunoprecipitated fragments to produce cDNA using SuperScript III First-Strand
808 Synthesis SuperMix (Thermo Fisher Scientific; catalog #11752050). We then performed
809 a preamplification reaction (14 cycles) using TaqMan PreAmp Master Mix (Thermo Fisher
810 Scientific; catalog #4384267), with a pooled-assay mix generated according to user
811 guidelines. Finally, best-coverage TaqMan Gene Expression Assays (see Supp. Figure
812 3) were run as per the manufacturer's instructions using the Bio Rad CFX Connect Real
813 Time system and software.

814

815 *Statistical Analysis*

816 All immunohistochemical and qPCR data were analyzed for using a 2 (male vs.
817 female) x 6 (P1 vs. P4 vs. P7 vs. P14 vs. P35 vs. Adult) between-subject factorial
818 analyses of variance (ANOVA) design using IBM SPSS Statistics (Version 20.0). Because
819 the treatment differed in males and females, for the organizational hormones study we
820 employed a one-way ANOVA to determine overall significance. Post-hoc analysis using
821 Bonferroni correction of pairwise comparisons for non-orthogonal comparisons were
822 conducted when $p<0.05$. We re-ran all of the statistics including litter composition (male
823 vs. female) as a covariate and found no significant effects of litter on any of the variables
824 measured (data not shown).

825 *RNAseq data analysis.* Sequencing reads were mapped to the mouse genome
826 (GRCm38.p5) and the Ensembl (releas-84) transcriptome annotation, using HISAT2
827 (Pertea et al., 2016). The mapping rates ranged from 74% to 95%. This resulted in a
828 number of mapped pairs from ~19.5 million up to 40 million (see Supplementary Table 6
829 for more details). The resulting SAM files were converted to BAM formant using
830 SAMtools[67]. The gene expression levels as counts were estimated using featureCounts[68]
831 with the following options: -t exon; -g gene_id; -F "GTF"; -B; -s 0; -p; -a. Counts from
832 technical replicates were added. Raw read counts were then filtered requiring more than
833 1 CPM (counts per million) in at least 25% of the samples and 16208 survived the filter
834 and were considered for further analysis. We next used the sva Bioconductor package
835 (Leek et al., 2012) to identify and correct for latent variables. Hierarchical clustering (using
836 the genes with a sd in expression level above the 95%) pre- and post sva correction show
837 the sample-to-sample relationship and relative clustering (see Supplemental Figure 2).
838 FastQC v0.10.1 and RNA-SeQC (v1.1.8) were used for QC (see Supplemental Table
839 QC). The edgeR function rpkm was used to estimate gene expression levels as RPKM.

840 *Differential expression analysis.* Differential expressed genes were then inferred
841 using the edgeR pipeline[69], using the trended dispersion to estimate the biological
842 variance and the GLM capability of the package. Nominal p-values from differential

843 expression analysis were FDR corrected, and an FDR cut-off of 0.05 was used for all the
844 tests.

845 *Functional enrichment analysis.* ConsensusPathDB[70] was used to test
846 differentially expressed genes for overrepresentation in Gene Ontologies and Canonical
847 Pathways.

848 *Weighted gene co-expression network analysis.* We used Weighted Gene Co-
849 expression Network Analysis (WGCNA)[71] for co-expression network analysis using gene
850 expression estimates (as log2(RPKM+1)), separately, from the 25 male samples and the
851 26 female samples, after cqn and sva correction. We estimated male and female co-
852 expression networks and modules using the function blockwiseModule, using the bicorr
853 as correlation estimate, a "signed" network type and a minModuleSize=50. The power
854 cut-off was set to 16 for both sets. The analysis produced a male network of 13 modules
855 and a female network of 15 modules, including the grey module of unassigned genes
856 (See WGCNA Summary Data).

857 *Transcription Factor Analysis.* We used the ChEA3 online suite (Keenan et al.,
858 2019) to test each network module for enrichment in Transcription Factors (TFs),
859 retaining only significant calls at FDR<0.05. We considered all the available databases
860 within ChEA3. This resulted in duplicated significant TFs, which were combined,
861 considering the union of all the reported target genes. We estimate the activity for each
862 TF using the camera gene set enrichment analysis algorithm (Wu and Smyth, 2012).
863 considering the P4 vs P1 difference. FDR corrected for multiple comparisons and used
864 FDR<0.05 as cut-off. Any TF estimated as non-significantly active was not retained for
865 further analysis. We then built a directed network from the remaining TFs, using the
866 known TF-target interaction and the WGCNA adjacency as edge weights.
867
868
869
870

References

1 Molyneaux, B. J., Arlotta, P., Menezes, J. R. L. & Macklis, J. D. Neuronal subtype specification in the cerebral cortex. *Nature Reviews Neuroscience* **8**, 427-437, doi:10.1038/nrn2151 (2007).

2 Barton, R. A. & Harvey, P. H. Mosaic evolution of brain structure in mammals. *Nature* **405**, 1055-1058, doi:10.1038/35016580 (2000).

3 Berry, M. & Rogers, A. W. The migration of neuroblasts in the developing cerebral cortex. *Journal of anatomy* **99**, 691-709 (1965).

4 Rakic, P. Mode of cell migration to the superficial layers of fetal monkey neocortex. *The Journal of Comparative Neurology* **145**, 61-83, doi:10.1002/cne.901450105 (1972).

5 Strakowski, S. M. *et al.* The functional neuroanatomy of bipolar disorder: a consensus model. *Bipolar Disorders* **14**, 313-325, doi:10.1111/j.1399-5618.2012.01022.x (2012).

6 Lin, C.-H. & Lane, H.-Y. Early Identification and Intervention of Schizophrenia: Insight From Hypotheses of Glutamate Dysfunction and Oxidative Stress. *Frontiers in psychiatry* **10**, 93, doi:10.3389/fpsyt.2019.00093 (2019).

7 Bayés, À. *et al.* Characterization of the proteome, diseases and evolution of the human postsynaptic density. *Nature Neuroscience* **14**, 19-21, doi:10.1038/nn.2719 (2011).

8 Bao, A.-M. & Swaab, D. F. Sexual differentiation of the human brain: Relation to gender identity, sexual orientation and neuropsychiatric disorders. *Frontiers in neuroendocrinology* **32**, 214-226, doi:10.1016/j.yfrne.2011.02.007 (2011).

9 Donner, N. C. & Lowry, C. A. Sex differences in anxiety and emotional behavior. *Pflugers Archiv : European journal of physiology* **465**, 601-626, doi:10.1007/s00424-013-1271-7 (2013).

10 Jaric, I., Rocks, D., Cham, H., Herchek, A. & Kundakovic, M. Sex and Estrous Cycle Effects on Anxiety- and Depression-Related Phenotypes in a Two-Hit Developmental Stress Model. *Frontiers in molecular neuroscience* **12**, 74, doi:10.3389/fnmol.2019.00074 (2019).

11 Kokras, N. *et al.* Forced swim test: What about females? *Neuropharmacology* **99**, 408-421, doi:10.1016/J.NEUROPHARM.2015.03.016 (2015).

12 McEwen, B. S., Lieberburg, I., Chaptal, C. & Krey, L. C. Aromatization: Important for sexual differentiation of the neonatal rat brain. *Hormones and Behavior* **9**, 249-263, doi:10.1016/0018-506X(77)90060-5 (1977).

13 Wright, C. L., Schwarz, J. S., Dean, S. L. & McCarthy, M. M. Cellular mechanisms of estradiol-mediated sexual differentiation of the brain. *Trends in Endocrinology & Metabolism* **21**, 553-561, doi:10.1016/j.tem.2010.05.004 (2010).

14 GORSKI, R. A. & WAGNER, J. W. Gonadal Activity and Sexual Differentiation of the Hypothalamus. *Endocrinology* **76**, 226-239, doi:10.1210/endo-76-2-226 (1965).

15 Johnson, R. T., Breedlove, S. M. & Jordan, C. L. Androgen receptors mediate masculinization of astrocytes in the rat posterodorsal medial amygdala during puberty. *The Journal of comparative neurology* **521**, 2298-2309, doi:10.1002/cne.23286 (2013).

16 Woolley, C. S., Gould, E., Frankfurt, M. & McEwen, B. S. Naturally occurring fluctuation in dendritic spine density on adult hippocampal pyramidal neurons. *Journal of Neuroscience* **10** (1990).

17 Bowers, J. M., Waddell, J. & Mccarthy, M. M. A developmental sex difference in hippocampal neurogenesis is mediated by endogenous oestradiol. *Biology of Sex Differences* **1**, 8, doi:10.1186/2042-6410-1-8 (2010).

18 Frazier, T. W., Georgiades, S., Bishop, S. L. & Hardan, A. Y. Behavioral and Cognitive Characteristics of Females and Males With Autism in the Simons Simplex Collection. *Journal of the American Academy of Child & Adolescent Psychiatry* **53**, 329-340.e323, doi:10.1016/J.JAAC.2013.12.004 (2014).

19 Parellada, M., Gomez-Vallejo, S., Burdeus, M. & Arango, C. Developmental Differences Between Schizophrenia and Bipolar Disorder. *Schizophrenia Bulletin* **43**, 1176-1189, doi:10.1093/schbul/sbx126 (2017).

20 Sloan, S. A. & Barres, B. A. Mechanisms of astrocyte development and their contributions to neurodevelopmental disorders. *Current opinion in neurobiology* **27**, 75-81, doi:10.1016/j.conb.2014.03.005 (2014).

21 Clarke, L. E. & Barres, B. A. Emerging roles of astrocytes in neural circuit development. *Nature Reviews Neuroscience* **14**, 311-321, doi:10.1038/nrn3484 (2013).

22 Loo, L. *et al.* Single-cell transcriptomic analysis of mouse neocortical development. *Nature communications* **10**, 134-134, doi:10.1038/s41467-018-08079-9 (2019).

23 Bayraktar, O. A. *et al.* Single-cell in situ transcriptomic map of astrocyte cortical layer diversity. *bioRxiv*, 432104, doi:10.1101/432104 (2018).

24 Anthony, T. E., Klein, C., Fishell, G. & Heintz, N. Radial Glia Serve as Neuronal Progenitors in All Regions of the Central Nervous System. *Neuron* **41**, 881-890, doi:10.1016/S0896-6273(04)00140-0 (2004).

25 Bi, B. *et al.* Cortical glial fibrillary acidic protein-positive cells generate neurons after perinatal hypoxic injury. *The Journal of neuroscience : the official journal of the Society for Neuroscience* **31**, 9205-9221, doi:10.1523/JNEUROSCI.0518-11.2011 (2011).

26 Ganat, Y. M. *et al.* Early Postnatal Astroglial Cells Produce Multilineage Precursors and Neural Stem Cells In Vivo. *Journal of Neuroscience* **26**, 8609-8621, doi:10.1523/JNEUROSCI.2532-06.2006 (2006).

27 Salmaso, N., Tomasi, S. & Vaccarino, F. M. Neurogenesis and maturation in neonatal brain injury. *Clinics in perinatology* **41**, 229-239, doi:10.1016/j.clp.2013.10.007 (2014).

28 Sofroniew, M. V. & Vinters, H. V. Astrocytes: biology and pathology. *Acta neuropathologica* **119**, 7-35, doi:10.1007/s00401-009-0619-8 (2010).

29 Chever, O., Pannasch, U., Ezan, P. & Rouach, N. Astroglial connexin 43 sustains glutamatergic synaptic efficacy. *Philosophical Transactions of the Royal Society of London B: Biological Sciences* **369** (2014).

30 Diniz, L. P. *et al.* Astrocyte transforming growth factor beta 1 promotes inhibitory synapse formation via CaM kinase II signaling. *Glia* **62**, 1917-1931, doi:10.1002/glia.22713 (2014).

31 Di Garbo, A., Barbi, M., Chillemi, S., Alloisio, S. & Nobile, M. Calcium signalling in astrocytes and modulation of neural activity. *Bio Systems* **89**, 74-83, doi:10.1016/j.biosystems.2006.05.013 (2007).

32 Cahoy, J. D. *et al.* A Transcriptome Database for Astrocytes, Neurons, and Oligodendrocytes: A New Resource for Understanding Brain Development and Function. *The Journal of Neuroscience* **28**, 264 LP-278, doi:10.1523/JNEUROSCI.4178-07.2008 (2008).

33 Milner, T. A. *et al.* Ultrastructural evidence that hippocampal alpha estrogen receptors are located at extranuclear sites. *Journal of Comparative Neurology* **429**, 355-371, doi:10.1002/1096-9861(20010115)429:3<355::AID-CNE1>3.0.CO;2-# 10.1002/1096-9861(20010115)429:33.0.CO;2-# (2001).

34 Platania, P. *et al.* Differential Expression of Estrogen Receptors Alpha and Beta in the Spinal Cord during Postnatal Development: Localization in Glial Cells. *Neuroendocrinology* **77**, 334-340, doi:10.1159/000070899 (2003).

35 Lee, E. *et al.* GPR30 regulates glutamate transporter GLT-1 expression in rat primary astrocytes. *The Journal of biological chemistry* **287**, 26817-26828, doi:10.1074/jbc.M112.341867 (2012).

36 Piechota, M. *et al.* Transcriptional signatures of steroid hormones in the striatal neurons and astrocytes. *BMC Neuroscience* **18**, 37, doi:10.1186/s12868-017-0352-5 (2017).

37 Acaz-Fonseca, E., Avila-Rodriguez, M., Garcia-Segura, L. M. & Barreto, G. E. Regulation of astroglia by gonadal steroid hormones under physiological and pathological conditions. *Progress in Neurobiology* **144**, 5-26, doi:10.1016/J.PNEUROBIO.2016.06.002 (2016).

38 Zhang, Y. *et al.* An RNA-sequencing transcriptome and splicing database of glia, neurons, and vascular cells of the cerebral cortex. *The Journal of neuroscience : the official journal of the Society for Neuroscience* **34**, 11929-11947, doi:10.1523/JNEUROSCI.1860-14.2014 (2014).

39 Scarr, E. *et al.* Increased cortical expression of the zinc transporter SLC39A12 suggests a breakdown in zinc cellular homeostasis as part of the pathophysiology of schizophrenia. *npj Schizophrenia* **2**, 16002, doi:10.1038/npjschz.2016.2 (2016).

40 Martinez-Garcia, A. *et al.* PLA2G3, a gene involved in oxidative stress induced death, is associated with Alzheimer's disease. *Journal of Alzheimer's disease : JAD* **22**, 1181-1187, doi:10.3233/jad-2010-101348 (2010).

41 Yaguchi, H. *et al.* TRIM67 protein negatively regulates Ras activity through degradation of 80K-H and induces neuritogenesis. *The Journal of biological chemistry* **287**, 12050-12059, doi:10.1074/jbc.M111.307678 (2012).

42 Aoki-Suzuki, M. *et al.* A family-based association study and gene expression analyses of netrin-G1 and -G2 genes in schizophrenia. *Biological psychiatry* **57**, 382-393, doi:10.1016/j.biopsych.2004.11.022 (2005).

43 Eastwood, S. L. & Harrison, P. J. Decreased mRNA expression of netrin-G1 and netrin-G2 in the temporal lobe in schizophrenia and bipolar disorder. *Neuropsychopharmacology : official publication of the American College of Neuropsychopharmacology* **33**, 933-945, doi:10.1038/sj.npp.1301457 (2008).

44 Bowers, J. M., Waddell, J. & McCarthy, M. M. A developmental sex difference in hippocampal neurogenesis is mediated by endogenous oestradiol. *Biology of Sex Differences* **1**, 8-8, doi:10.1186/2042-6410-1-8 (2010).

45 Lenz, K. M. & McCarthy, M. M. Organized for sex - steroid hormones and the developing hypothalamus. *The European journal of neuroscience* **32**, 2096-2104, doi:10.1111/j.1460-9568.2010.07511.x (2010).

46 Lenz, K. M. & McCarthy, M. M. Organized for sex - steroid hormones and the developing hypothalamus. *The European journal of neuroscience* **32**, 2096-2104, doi:10.1111/j.1460-9568.2010.07511.x (2010).

1003 47 Clarkson, J. & Herbison, A. E. Hypothalamic control of the male neonatal testosterone
1004 surge. *Philosophical transactions of the Royal Society of London. Series B, Biological*
1005 *sciences* **371**, 20150115, doi:10.1098/rstb.2015.0115 (2016).
1006 48 Swaab, D. F. Sexual differentiation of the brain and behavior. *Best Practice & Research*
1007 *Clinical Endocrinology & Metabolism* **21**, 431-444, doi:10.1016/j.beem.2007.04.003
1008 (2007).
1009 49 Salmaso, N. & Woodside, B. Fluctuations in astrocytic basic fibroblast growth factor in
1010 the cingulate cortex of cycling, ovariectomized and postpartum animals. *Neuroscience* **154**,
1011 932-939, doi:10.1016/J.NEUROSCIENCE.2008.03.063 (2008).
1012 50 Arnsten, A. F. T. Ameliorating prefrontal cortical dysfunction in mental illness: inhibition
1013 of phosphotidyl inositol-protein kinase C signaling. *Psychopharmacology* **202**, 445-455,
1014 doi:10.1007/s00213-008-1274-9 (2009).
1015 51 Oberlander, J. G. & Woolley, C. S. 17β-Estradiol Acutely Potentiates Glutamatergic
1016 Synaptic Transmission in the Hippocampus through Distinct Mechanisms in Males and
1017 Females. *The Journal of neuroscience : the official journal of the Society for Neuroscience*
1018 **36**, 2677-2690, doi:10.1523/JNEUROSCI.4437-15.2016 (2016).
1019 52 De Vries, G. J. Minireview: Sex Differences in Adult and Developing Brains:
1020 Compensation, Compensation, Compensation. *Endocrinology* **145**, 1063-1068,
1021 doi:10.1210/en.2003-1504 (2004).
1022 53 Mizukami, H. *et al.* KDM5D-mediated H3K4 demethylation is required for sexually
1023 dimorphic gene expression in mouse embryonic fibroblasts. *The Journal of Biochemistry*
1024 **165**, 335-342, doi:10.1093/jb/mvy106 (2018).
1025 54 Arnold, A. P. *et al.* Minireview: Sex Chromosomes and Brain Sexual Differentiation.
1026 *Endocrinology* **145**, 1057-1062, doi:10.1210/en.2003-1491 (2004).
1027 55 Galvez-Contreras, A. Y., Campos-Ordonez, T., Gonzalez-Castaneda, R. E. & Gonzalez-
1028 Perez, O. Alterations of Growth Factors in Autism and Attention-Deficit/Hyperactivity
1029 Disorder. *Frontiers in psychiatry* **8**, 126, doi:10.3389/fpsyt.2017.00126 (2017).
1030 56 Matute, C., Melone, M., Vallejo-Illarramendi, A. & Conti, F. Increased expression of the
1031 astrocytic glutamate transporter GLT-1 in the prefrontal cortex of schizophrenics. *Glia* **49**,
1032 451-455, doi:10.1002/glia.20119 (2005).
1033 57 Mayoral, S. R., Omar, G. & Penn, A. A. Sex differences in a hypoxia model of preterm
1034 brain damage. *Pediatric research* **66**, 248-253, doi:10.1203/PDR.0b013e3181b1bc34
1035 (2009).
1036 58 van der Kooij, M. A. *et al.* Mild neonatal hypoxia–ischemia induces long-term motor- and
1037 cognitive impairments in mice. *Brain, Behavior, and Immunity* **24**, 850-856,
1038 doi:https://doi.org/10.1016/j.bbi.2009.09.003 (2010).
1039 59 Gerstner, B. *et al.* 17beta-estradiol protects against hypoxic/ischemic white matter damage
1040 in the neonatal rat brain. *Journal of neuroscience research* **87**, 2078-2086,
1041 doi:10.1002/jnr.22023 (2009).
1042 60 Salmaso, N. *et al.* Environmental enrichment increases the GFAP+ stem cell pool and
1043 reverses hypoxia-induced cognitive deficits in juvenile mice. *The Journal of neuroscience*
1044 *: the official journal of the Society for Neuroscience* **32**, 8930-8939,
1045 doi:10.1523/JNEUROSCI.1398-12.2012 (2012).
1046 61 Gillies, G. E. & McArthur, S. Estrogen actions in the brain and the basis for differential
1047 action in men and women: a case for sex-specific medicines. *Pharmacological reviews* **62**,
1048 155-198, doi:10.1124/pr.109.002071 (2010).

1049 62 Bowen, R. S., Ferguson, D. P. & Lightfoot, J. T. Effects of Aromatase Inhibition on the
1050 Physical Activity Levels of Male Mice. *Journal of steroids & hormonal science* **1**, 1-7,
1051 doi:10.4172/2157-7536.S1-001 (2011).
1052 63 Komitova, M. *et al.* Hypoxia-induced developmental delays of inhibitory interneurons are
1053 reversed by environmental enrichment in the postnatal mouse forebrain. *The Journal of*
1054 *neuroscience : the official journal of the Society for Neuroscience* **33**, 13375-13387,
1055 doi:10.1523/JNEUROSCI.5286-12.2013 (2013).
1056 64 Salmaso, N. *et al.* Contribution of maternal oxygenic state to the effects of chronic
1057 postnatal hypoxia on mouse body and brain development. *Neuroscience letters* **604**, 12-17,
1058 doi:10.1016/j.neulet.2015.07.033 (2015).
1059 65 Schmitz, C. & Hof, P. R. Design-based stereology in neuroscience. *Neuroscience* **130**, 813-
1060 831, doi:10.1016/j.neuroscience.2004.08.050 (2005).
1061 66 Simard, S. *et al.* Profiling changes in cortical astroglial cells following chronic stress.
1062 *Neuropsychopharmacology : official publication of the American College of*
1063 *Neuropsychopharmacology* **43**, 1961-1971, doi:10.1038/s41386-018-0105-x (2018).
1064 67 Li, H. *et al.* The Sequence Alignment/Map format and SAMtools. *Bioinformatics (Oxford,*
1065 *England)* **25**, 2078-2079, doi:10.1093/bioinformatics/btp352 (2009).
1066 68 Liao, Y., Smyth, G. K. & Shi, W. featureCounts: an efficient general purpose program for
1067 assigning sequence reads to genomic features. *Bioinformatics (Oxford, England)* **30**, 923-
1068 930, doi:10.1093/bioinformatics/btt656 (2014).
1069 69 Robinson, M. D., McCarthy, D. J. & Smyth, G. K. edgeR: a Bioconductor package for
1070 differential expression analysis of digital gene expression data. *Bioinformatics (Oxford,*
1071 *England)* **26**, 139-140, doi:10.1093/bioinformatics/btp616 (2010).
1072 70 Kamburov, A., Stelzl, U., Lehrach, H. & Herwig, R. The ConsensusPathDB interaction
1073 database: 2013 update. *Nucleic acids research* **41**, D793-800, doi:10.1093/nar/gks1055
1074 (2013).
1075 71 Langfelder, P. & Horvath, S. WGCNA: an R package for weighted correlation network
1076 analysis. *BMC Bioinformatics* **9**, 559-559, doi:10.1186/1471-2105-9-559 (2008).

1077

1078

1079 ***Figure Captions***
1080
1081 Figure 1. A- Total number of eGFP+ cells in the neocortex. B- Estimated neocortical
1082 volume. C- Percentage of radial-like eGFP+ cells. * indicates a significant difference
1083 from all other time points. Bars denote group mean and error bars displayed are ± SEM.
1084
1085 Figure 2. A- Clustered heat map of individual sample gene expression levels from
1086 TRAPseq data. B- Represents a heat map of samples manually sorted by sex and age.
1087
1088 Figure 3. A- Total number of cells expressing GFAP. B- Total number of vimentin+ cells.
1089 C- Percent GFP+ co-expressing Ki67. D- Representative mosaic of confocal
1090 pictomicrographs at 10x, whole cortex sagittal section (left), zoom on the molecular
1091 layer (right). * indicates a significant difference from all other time points; # indicates a
1092 significant difference between male and female at that time point. Bars denote group
1093 mean and error bars displayed are ± SEM.
1094
1095 Figure 4. A- Number of DEGs between early and late phenotype in males and females.
1096 B- Venn diagram displaying overlap in DEGs between females and males. C- Bar plot
1097 showing the number of up- and downregulated DEGs between males and females at
1098 each time point (females=reference group). D- Bar plot showing the number of DEGs
1099 between time points.
1100
1101 Figure 5- Plot of modules Eigen-value vs time. Represented is the subset of the male
1102 and female modules enriched in astrocyte subtype markers. . A- modules enriched in
1103 AST1, AST2, AST3 subtypes; top row: modules M2, M3, M12; bottom row: F3, F9. B-
1104 modules enriched in AST4 subtypes; top row: modules M8, M11, M1; bottom row: F6,
1105 F2, F10. C- modules enriched in AST5 subtypes; top row: modules M2, M6, M1; bottom
1106 row: F3, F9.
1107
1108 Figure 6. A- Density of COX2+ GFP+ astroglial cells in the cortex across examined
1109 timepoints. Bars represent group means, error bars are displayed as ± SEM.
1110 Representative mosaic reconstruction of Cox2, eGFP staining in a male and female
1111 mouse within the PFC region of the cortex at P1 (top). A 63X+oil image highlighting a
1112 Cox2+, eGFP+ astroglia (white arrow) and a Cox2-, eGFP+ astroglia (pink arrow) in the
1113 PFC (bottom). B- top panel- Graphical illustration of arbitrary levels circulating gonadal
1114 hormones (testosterone, solid lines; estrogen, broken lines) in males (blue) and females
1115 (red) overlay with ages examined in the study. B- lower panel- important cortical
1116 neurulation events represented by colour saturation. Darker saturation indicates when a
1117 process is more active, lower saturation indicates when a process is less active.
1118 (Adapted from: Ellis 2004; Gillies and McArthur, 2010; Anderson, 2003; Estes and
1119 McAllistter, 2016). C- Density of of COX2+ cells in the cortex at P1 in males and
1120 females treated with estradiol or letrozole. Bars represent group means, error bars are
1121 displayed as ± SEM. * indicates significance between treatment and vehicle.

Figure 1

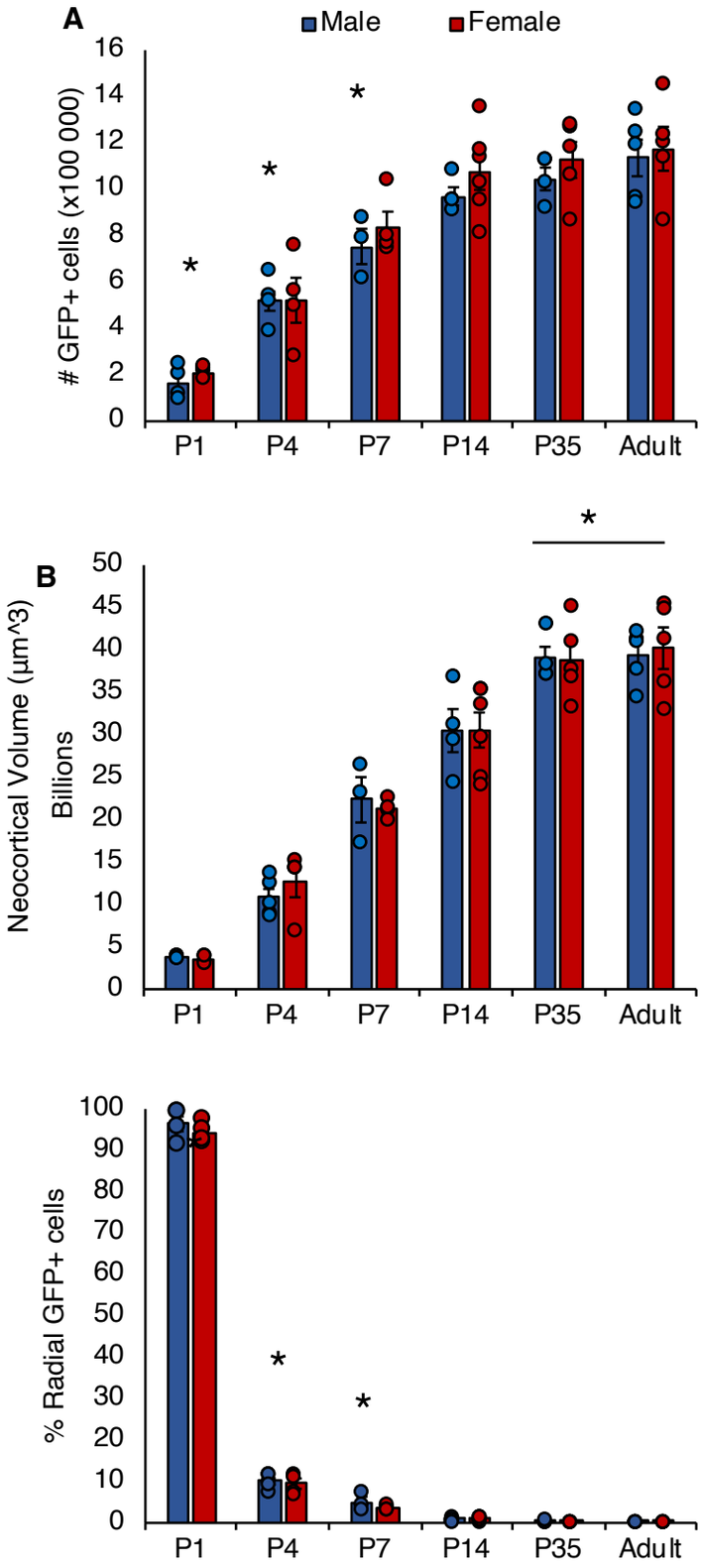
A
Male
Female
GFP+ cells (x100 000)
16
14
12
10
8
6
4
2
0
*
*
*
P1
P4
P7
P14
P35
Adult
B
Neocortical Volume (µm^3)
Billions
50
45
40
35
30
25
20
15
10
5
0
*
P1
P4
P7
P14
P35
Adult
% Radial GFP+ cells
100
90
80
70
60
50
40
30
20
10
0
*
*
P1
P4
P7
P14
P35
Adult

Figure 2

A

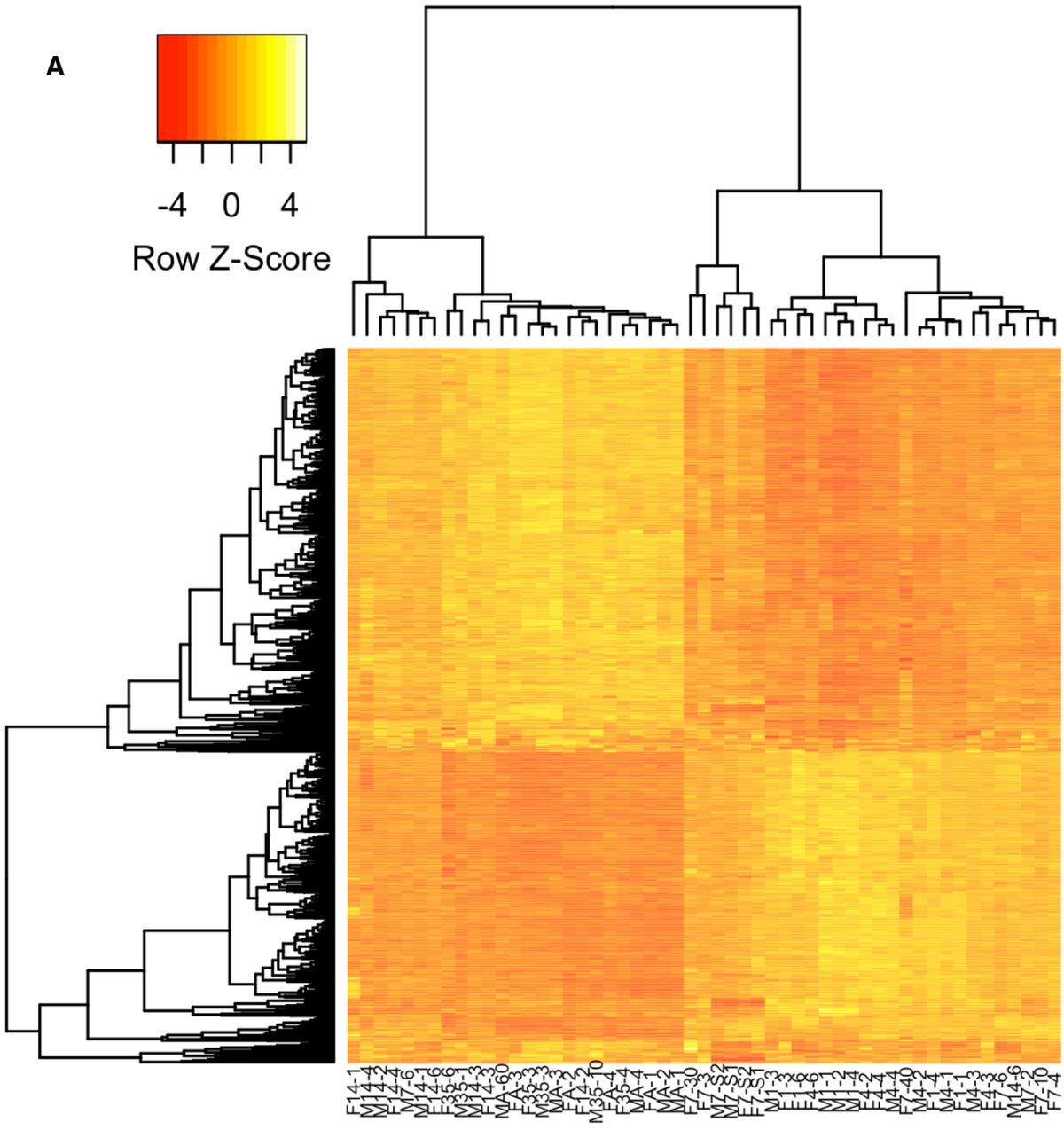
-4
0
4
Row Z-Score
F14-1
M14-4
M14-2
F14-4
M7-6
M14-1
F14-6
F35-6
M35-1
M14-3
MA-60
EA-3
F35-3
M35-3
MA-3
F14-2
F14-10
M35-4
F35-4
MA-1
FA-1
MA-2
F7-30
F7-3
M7-S2
M7-S1
F7-S2
F7-S1
M1-3
E1-3
E1-6
E4-6
M1-2
M1-4
E4-2
E4-4
M4-40
F7-40
M4-2
F1-4
M4-1
M4-3
E4-3
F7-6
M14-6
M7-2
F7-10
F7-4

B

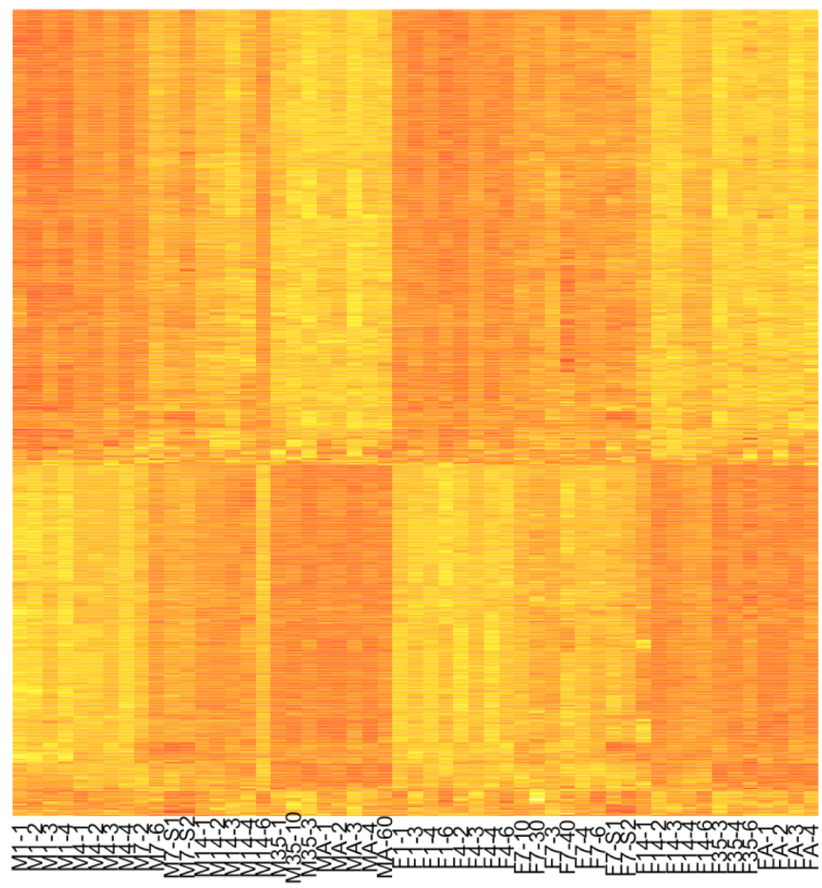
M1-1
M1-2
M1-3
M1-4
M4-2
M4-3
M4-4
M7-6
M7-S2
M7-S1
M14-1
M14-2
M14-3
M14-4
M14-6
M35-1
M35-10
M35-3
MA-1
MA-2
MA-3
MA-4
MA-60
E1-3
E1-4
E1-6
E4-3
E4-4
E4-6
F7-10
F7-30
F7-3
F7-40
F7-4
F7-6
F7-S1
F7-S2
F14-1
F14-2
F14-3
F14-4
F14-6
F35-3
F35-4
F35-6
EA-1
EA-2
EA-3
EA-4

Figure 3

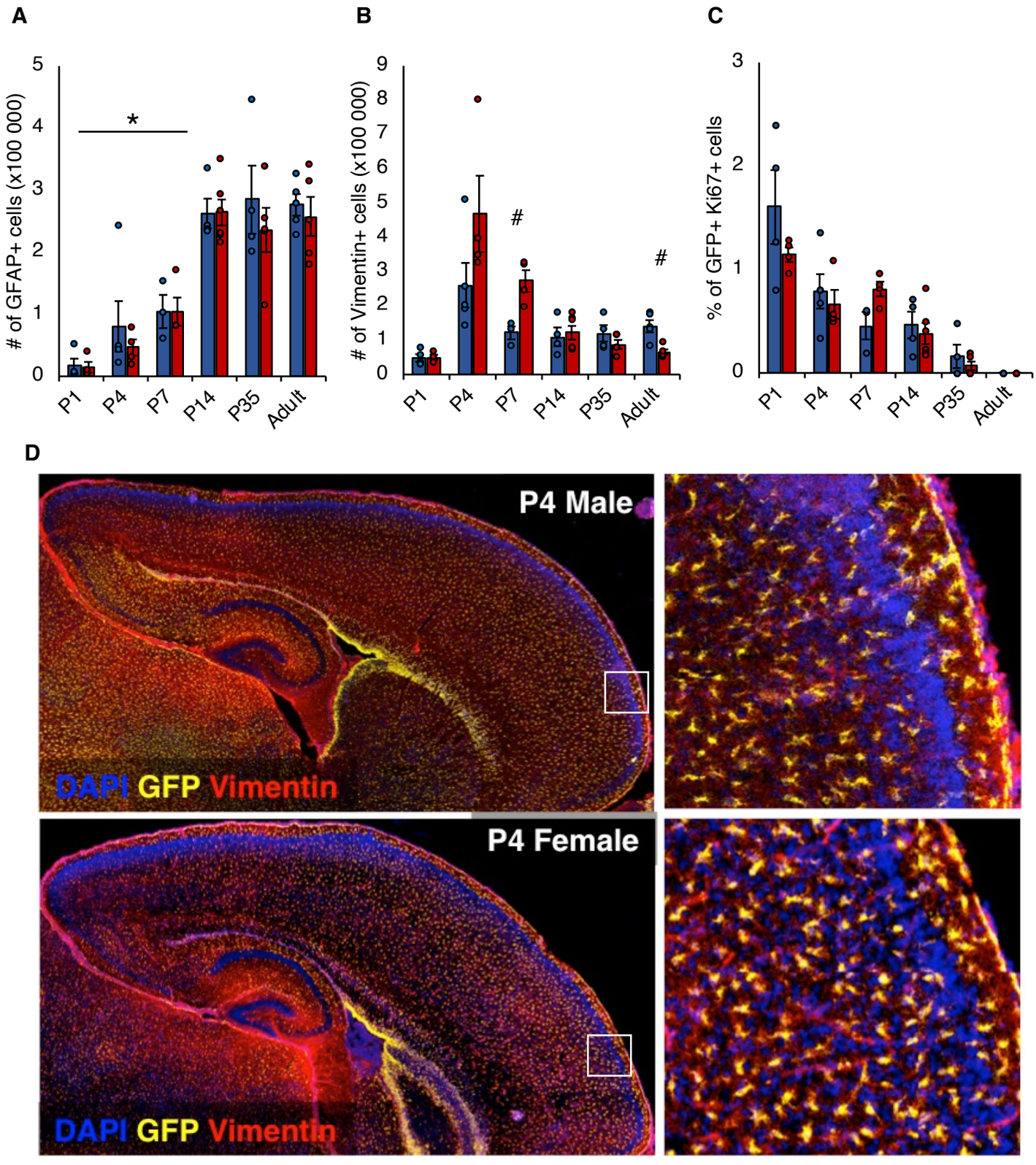
A
# of GFAP+ cells (x100 000)
*
P1
P4
P7
P14
P35
Adult
B
# of Vimentin+ cells (x100 000)
#
#
C
% of GFP+ Ki67+ cells
D
P4 Male
DAPI GFP Vimentin
P4 Female
DAPI GFP Vimentin

Figure 4

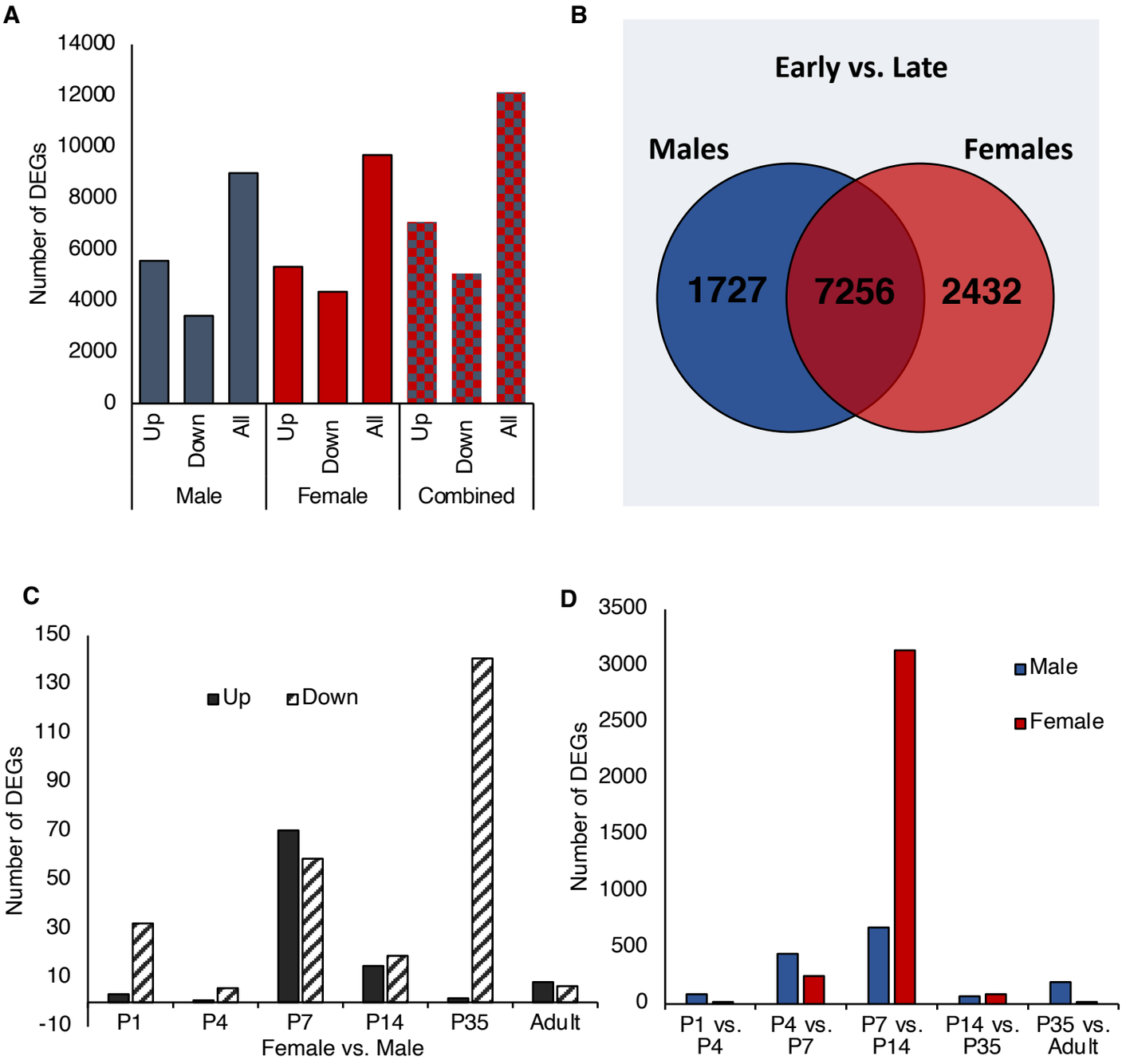
A
14000
12000
10000
8000
6000
4000
2000
0
Number of DEGs
Up
Down
All
Up
Down
All
Up
Down
All
Male
Female
Combined
B
Early vs. Late
Males
Females
1727
7256
2432
C
150
130
110
90
70
50
30
10
-10
Number of DEGs
Up
Down
P1
P4
P7
P14
P35
Adult
Female vs. Male
D
3500
3000
2500
2000
1500
1000
500
0
Number of DEGs
Male
Female
P1 vs. P4
P4 vs. P7
P7 vs. P14
P14 vs. P35
P35 vs. Adult

Figure 5

A-subtypes 1, 2 & 3

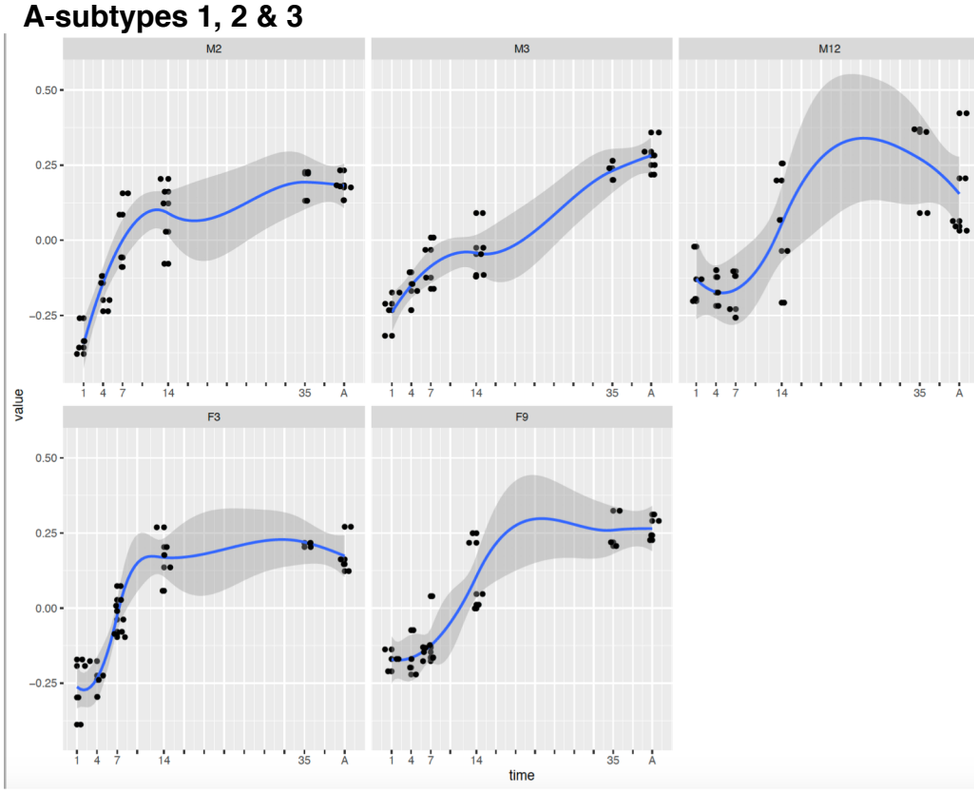

B- subtype 4

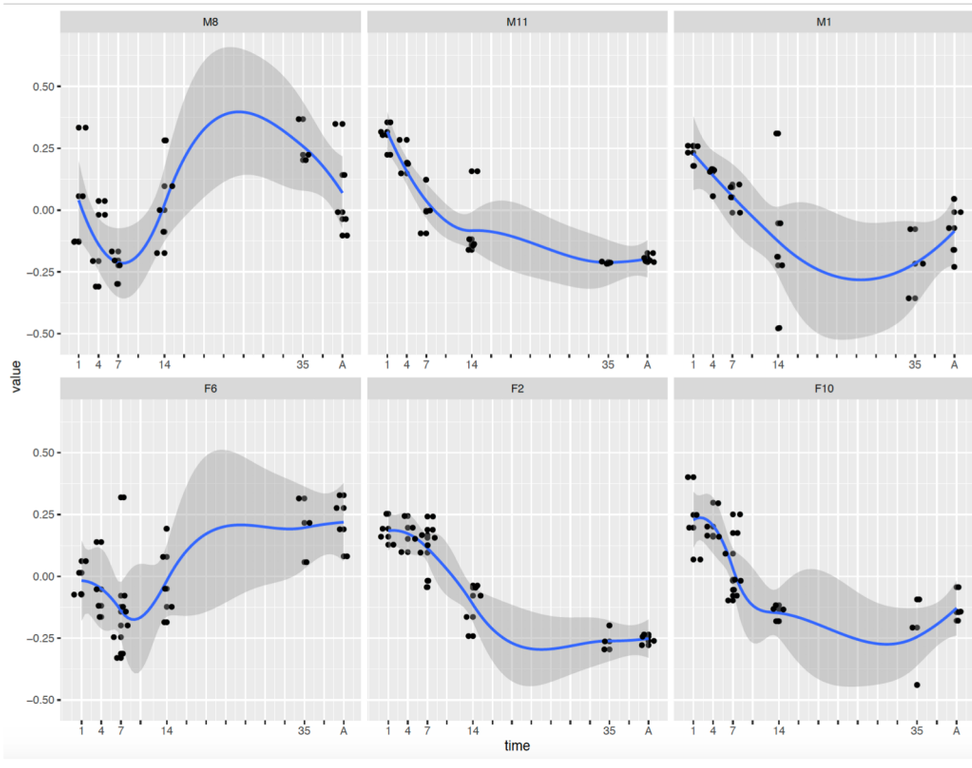

C- subtype 5

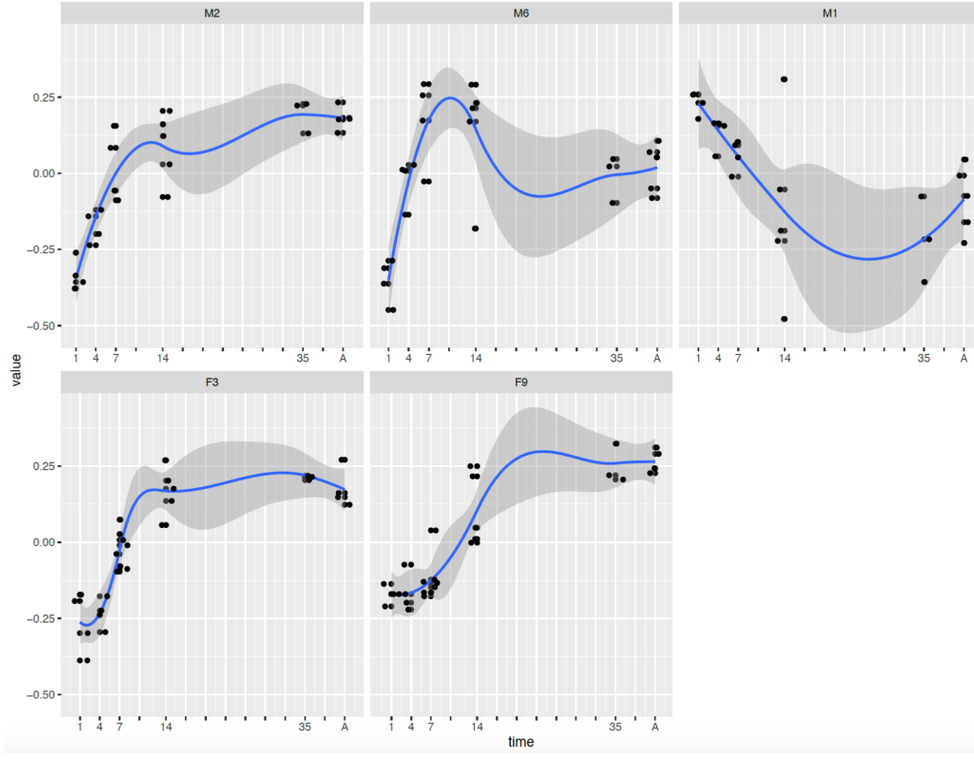

Figure 6

A

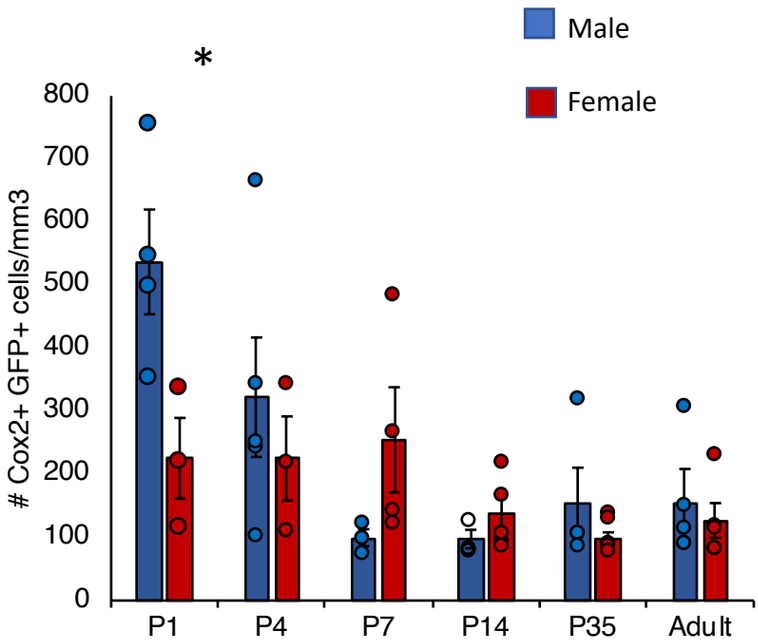
Male
Female
*
Cox2+ GFP+ cells/mm3
800
700
600
500
400
300
200
100
0
P1
P4
P7
P14
P35
Adult

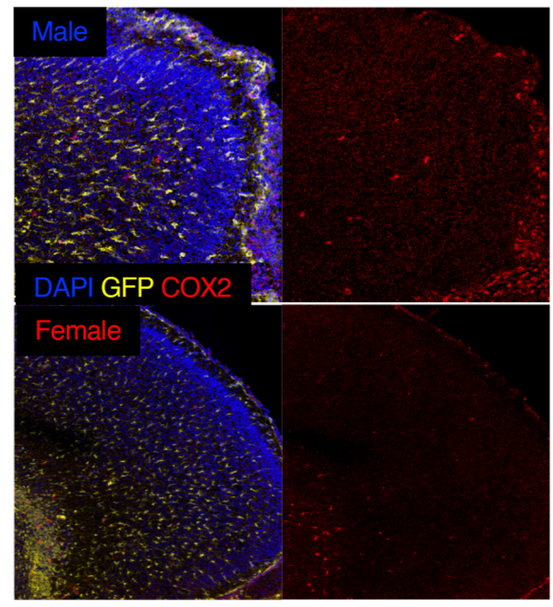
Male
DAPI GFP COX2
Female

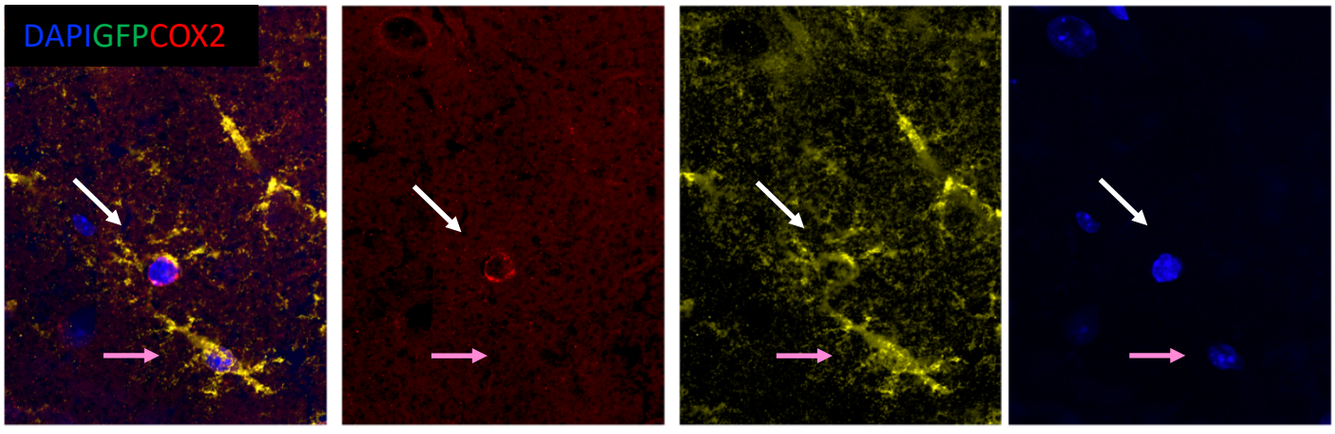
DAPIGFPCOX2

B

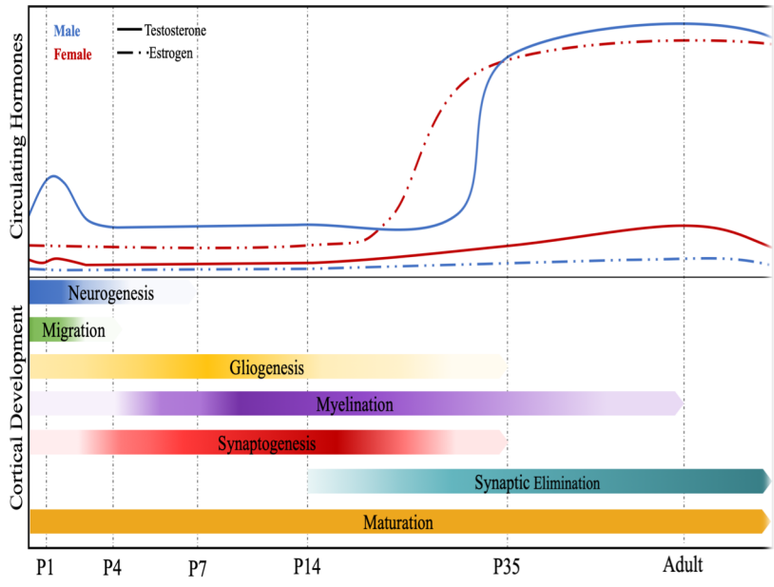
Male
Female
Testosterone
Estrogen
Circulating Hormones
Cortical Development
Neurogenesis
Migration
Gliogenesis
Myelination
Synaptogenesis
Synaptic Elimination
Maturation
P1
P4
P7
P14
P35
Adult

C

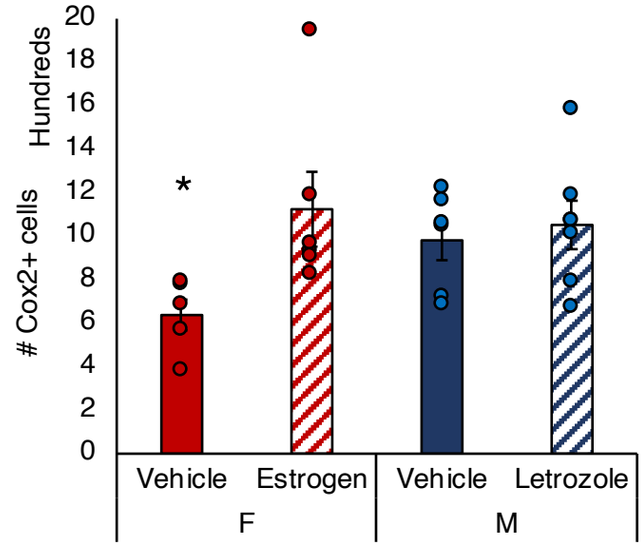
Hundreds
Cox2+ cells
20
18
16
14
12
10
8
6
4
2
0
*
Vehicle
Estrogen
Vehicle
Letrozole
F
M

Supplemental Figure 1

Animal numbers for immunohistochemistry

Age/Sex	P1*	P4	P7	P14	P35	Adult
M	4	5	3	4	4	5
F	4	4	4	6	5	5
Total	8	9	7	10	9	10

Animal numbers for TRAPseq

Age/Sex	P1*	P4	P7	P14	P35	Adult
M	4	4	4	5	3	5
F	4	4	8	5	3	4
Total	8	8	12	10	6	9

Animal numbers for organizational hormones study

Sex/Group	Vehicle	Estradiol/Letrozole
Male	6	7
Female	5	6

Antibodies used for immunohistochemistry

Antibody	Supplier	Species	Dilution
anti-GFP	Abcam (ab19370)	Chicken	1:1000
anti-GFAP	Abcam (ab134436)	Chicken	1:500
anti-GFAP	Abcam (ab10062)	Mouse	1:1000
anti-GFAP	Sigma (AB5804)	Rabbit	1:500
anti-GS	Abcam (ab73593)	Mouse	1:500
anti-Ki67	Invitrogen (PA1-21520)	Rabbit	1:500
anti-Vimentin	Invitrogen (PA5-27231)	Rabbit	1:500
Donkey anti-chicken	Alexafluor 488		1:1000
Donkey anti-mouse	Alexafluor 488		1:1000
Donkey anti-rabbit	Alexafluor 546		1:500
Donkey anti-mouse	Alexafluor 546		1:500

Supplemental Figure 2

A- Pre-correction

B- Post-correction

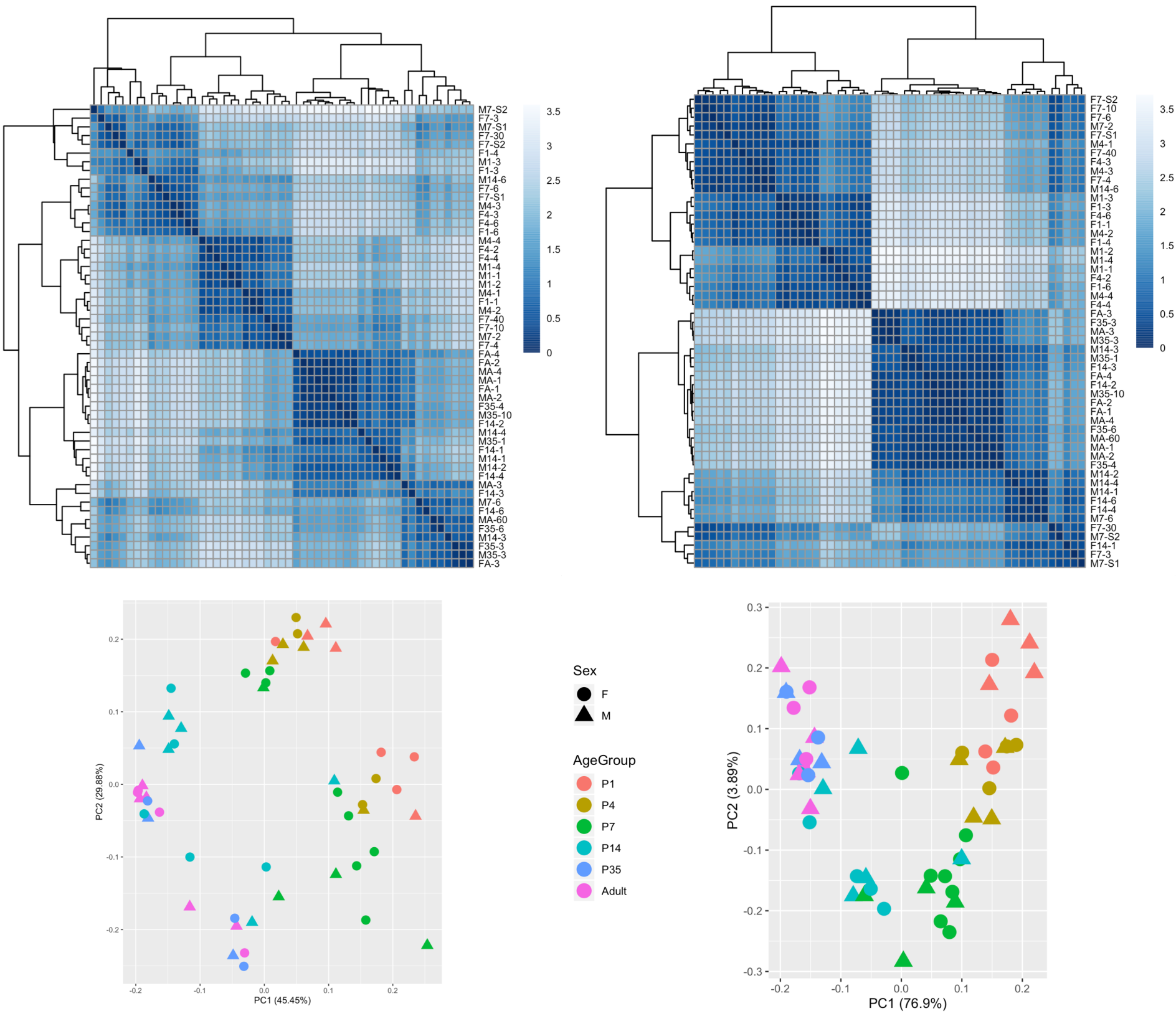

Top- Hierarchical clustering (using the genes with a sd in expression level above the 95%) pre- and post sva correction show the sample-to-sample relationship and relative clustering

Bottom- Principal component analysis plots. Represented are the sample distribution along the first principal component (PC1) and then second principal component (PC2). Shows in brackets os the percentage of the variance captured by PC1 and PC2. Circles: female samples; squares: male samples. Symbols are color coded by age.

Supplemental Figure 3

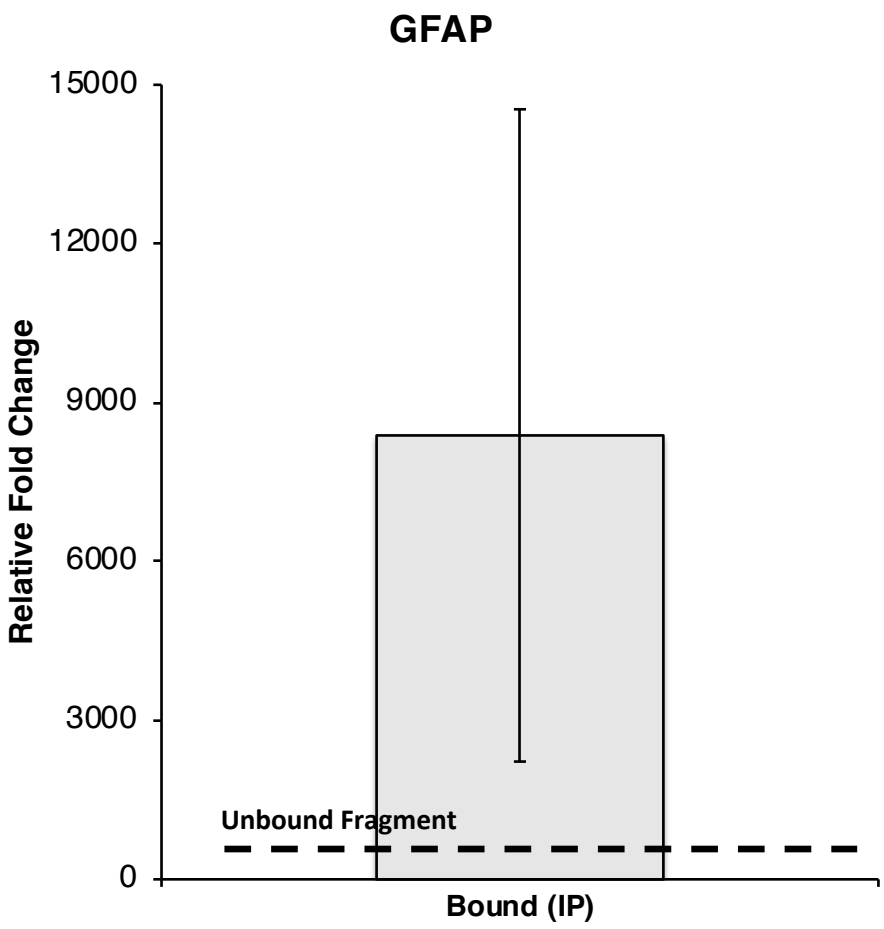

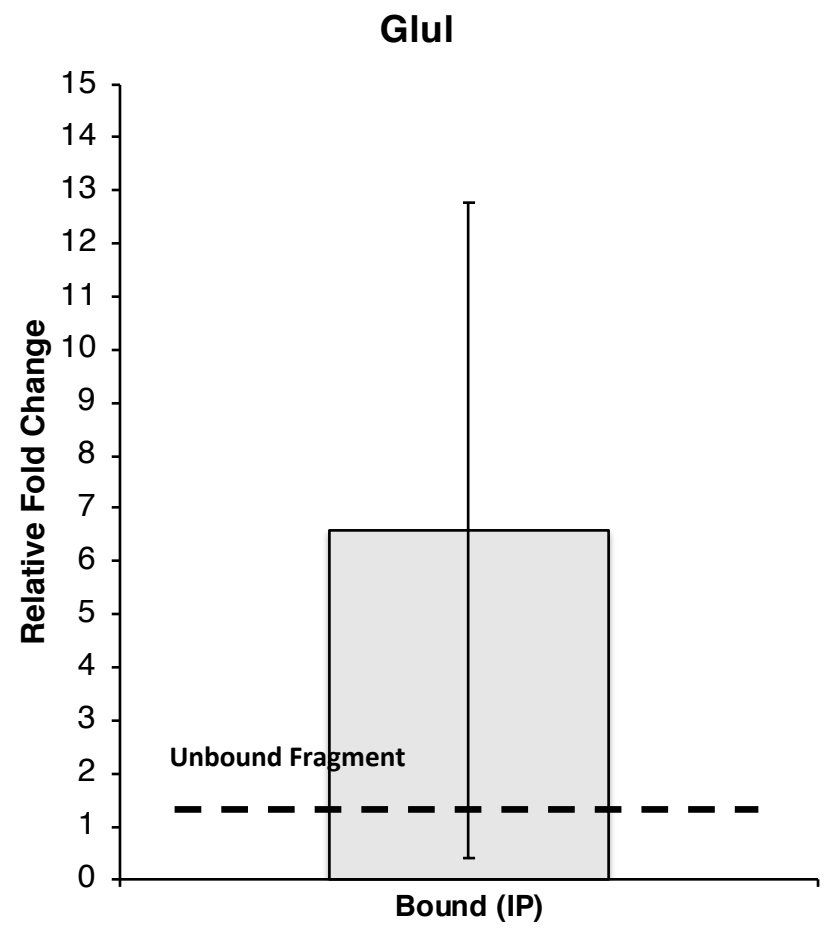

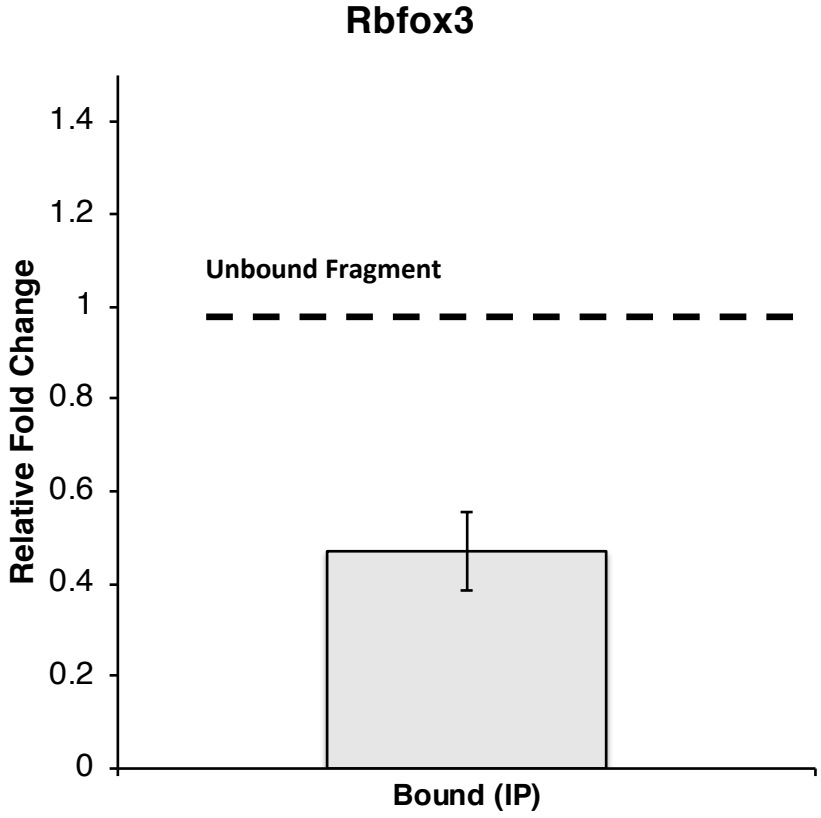

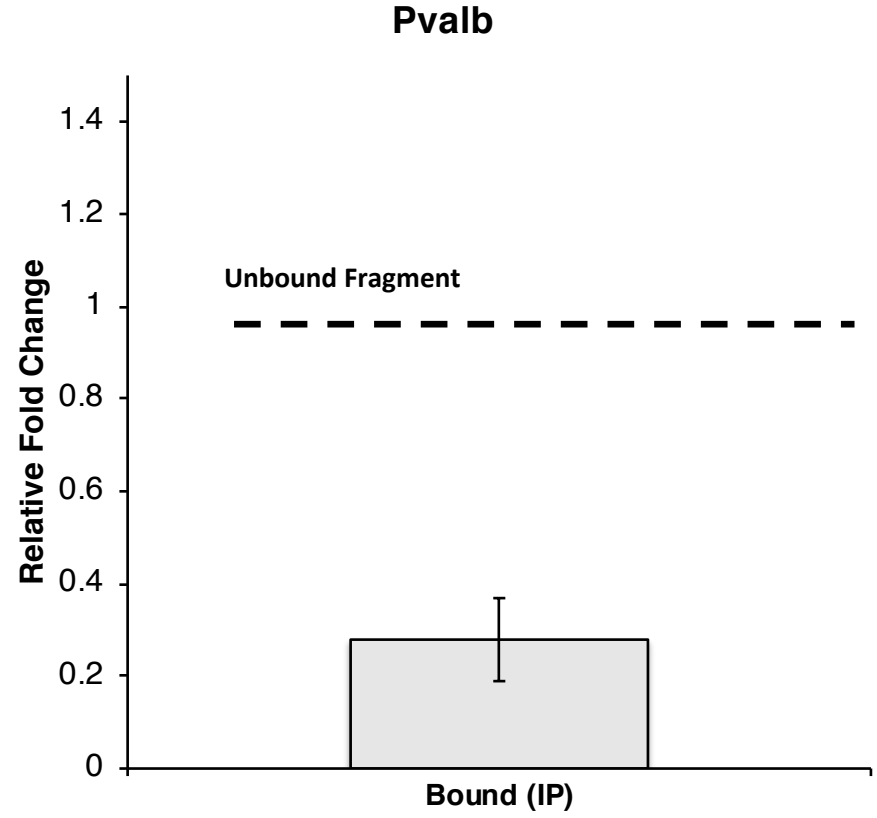

Supplemental Figure 4

Developmental Changes

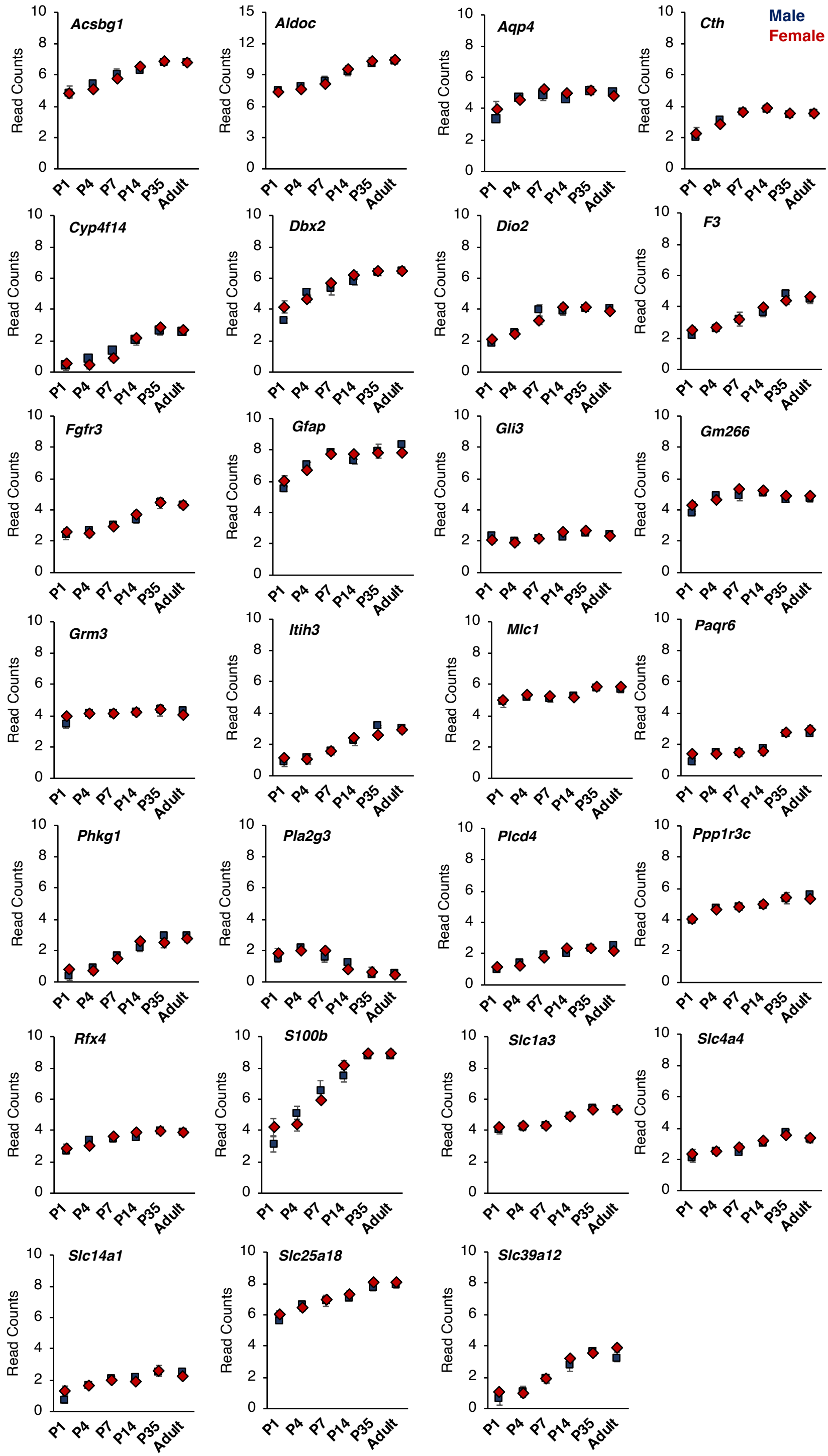

Supplemental Figure 5

Stable through Development

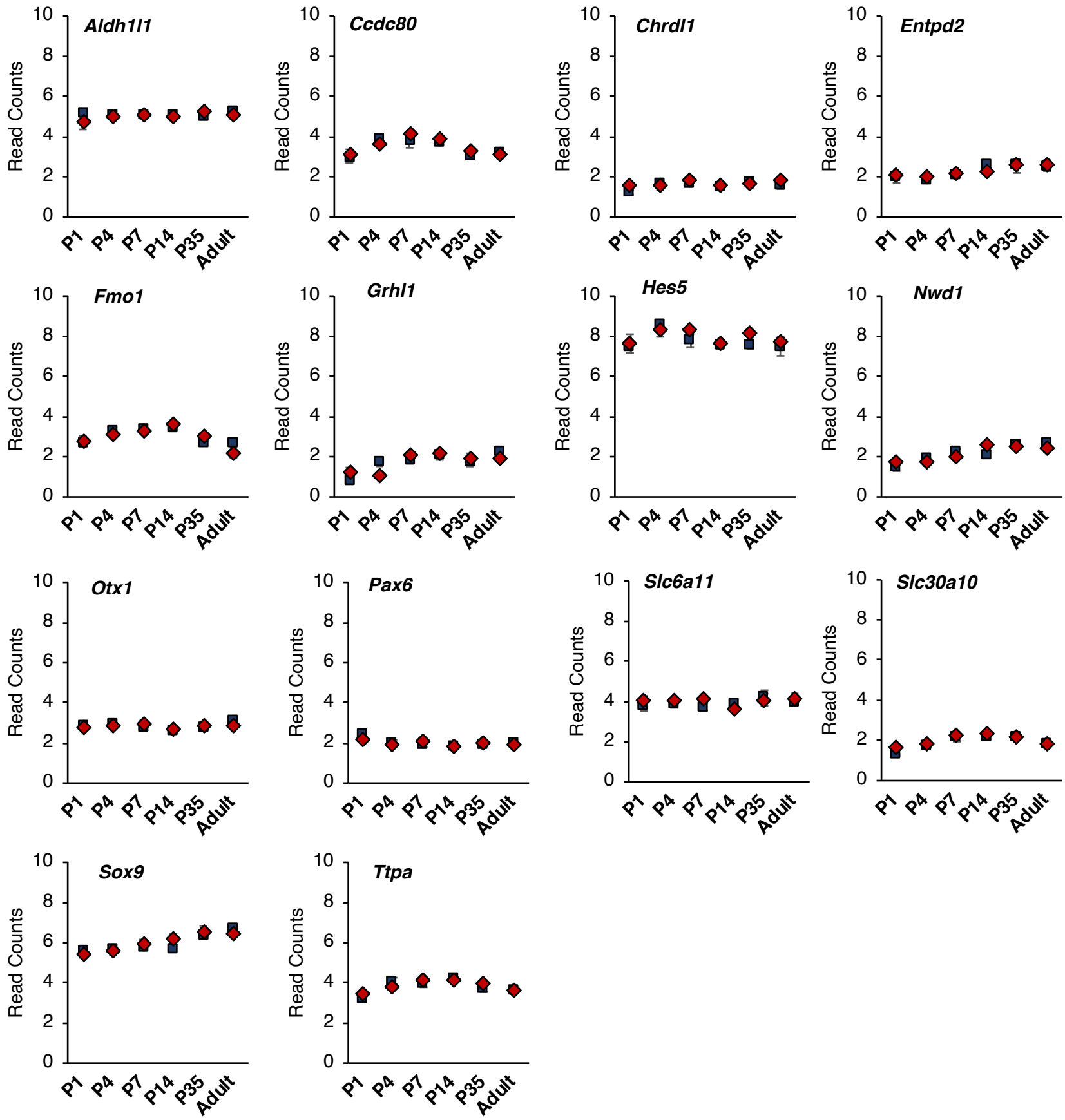

Supplemental Figure 6

Low Expression

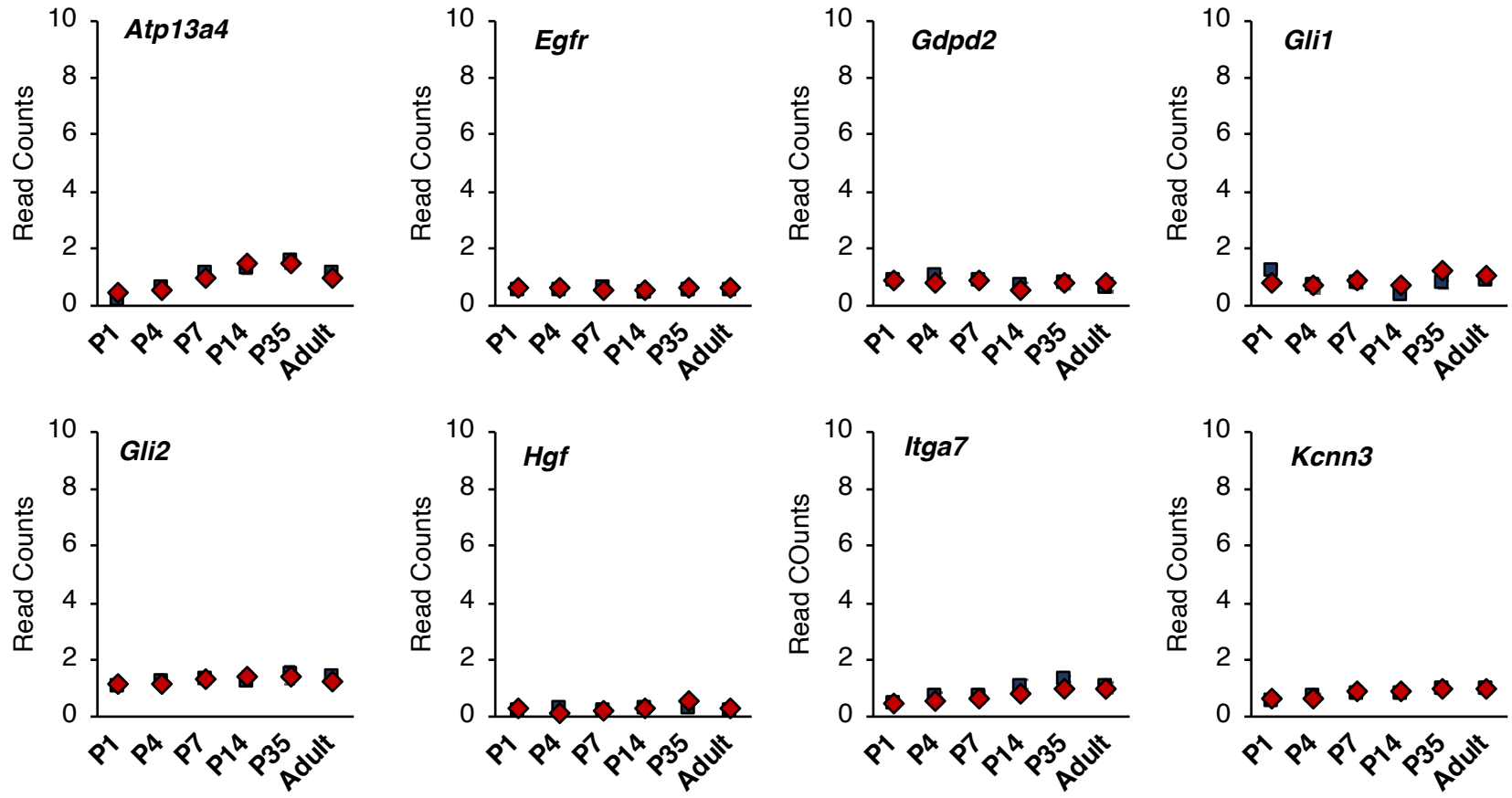

Supplemental Figure 7

Layers 2-4

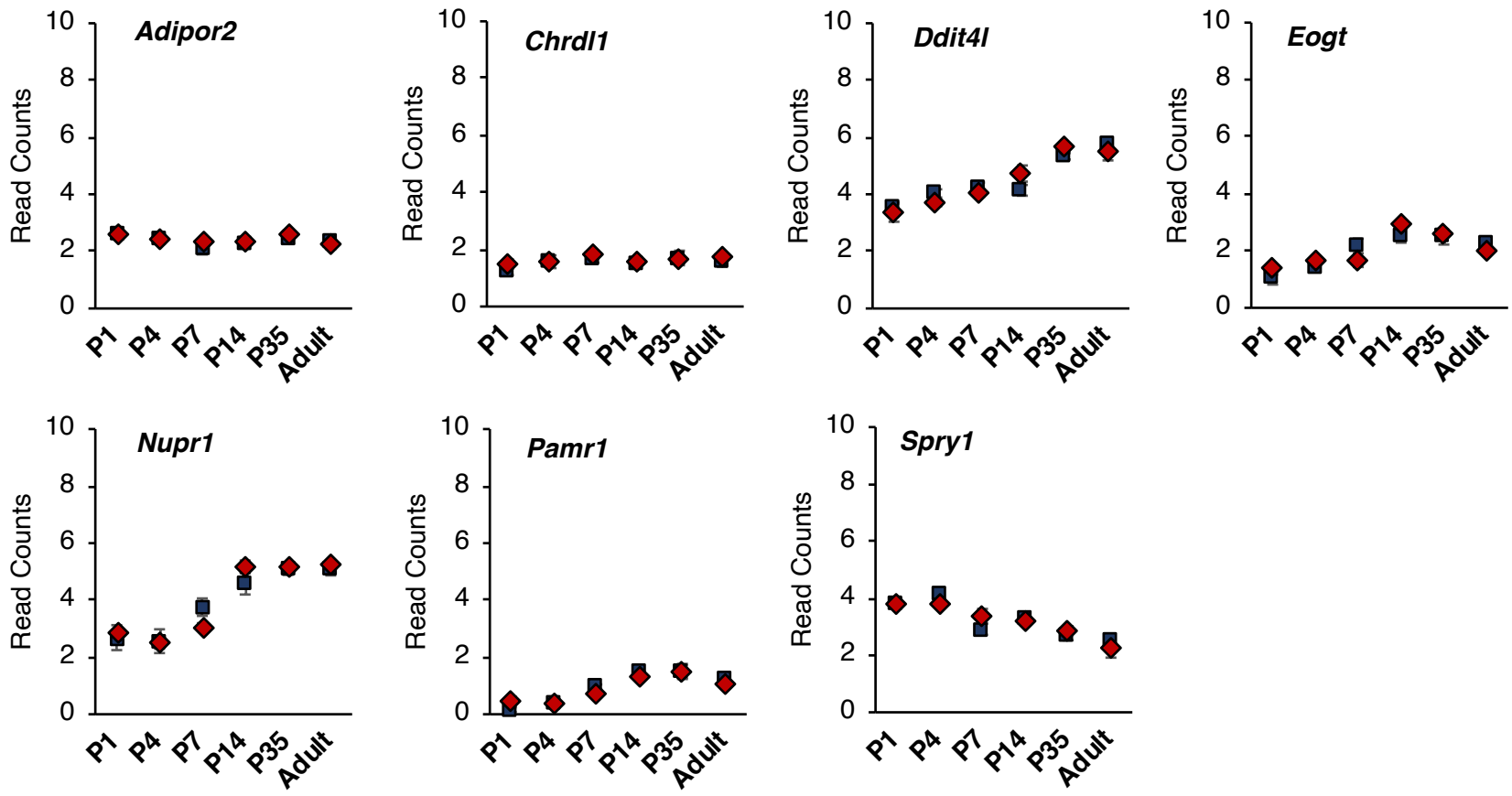

Deep Layers 5-6

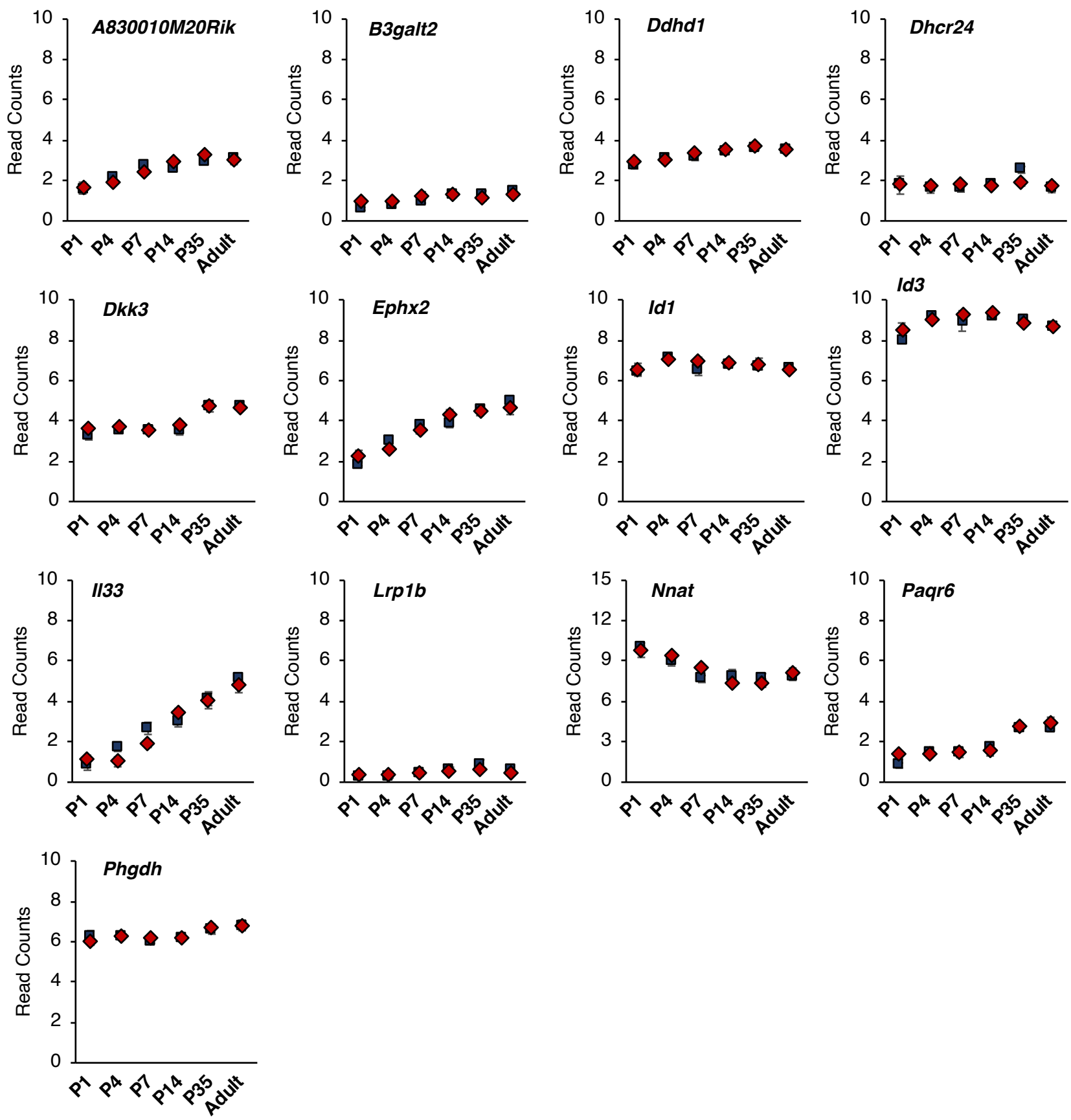

Supplemental Figure 8

Upper Biased but Pan Astro

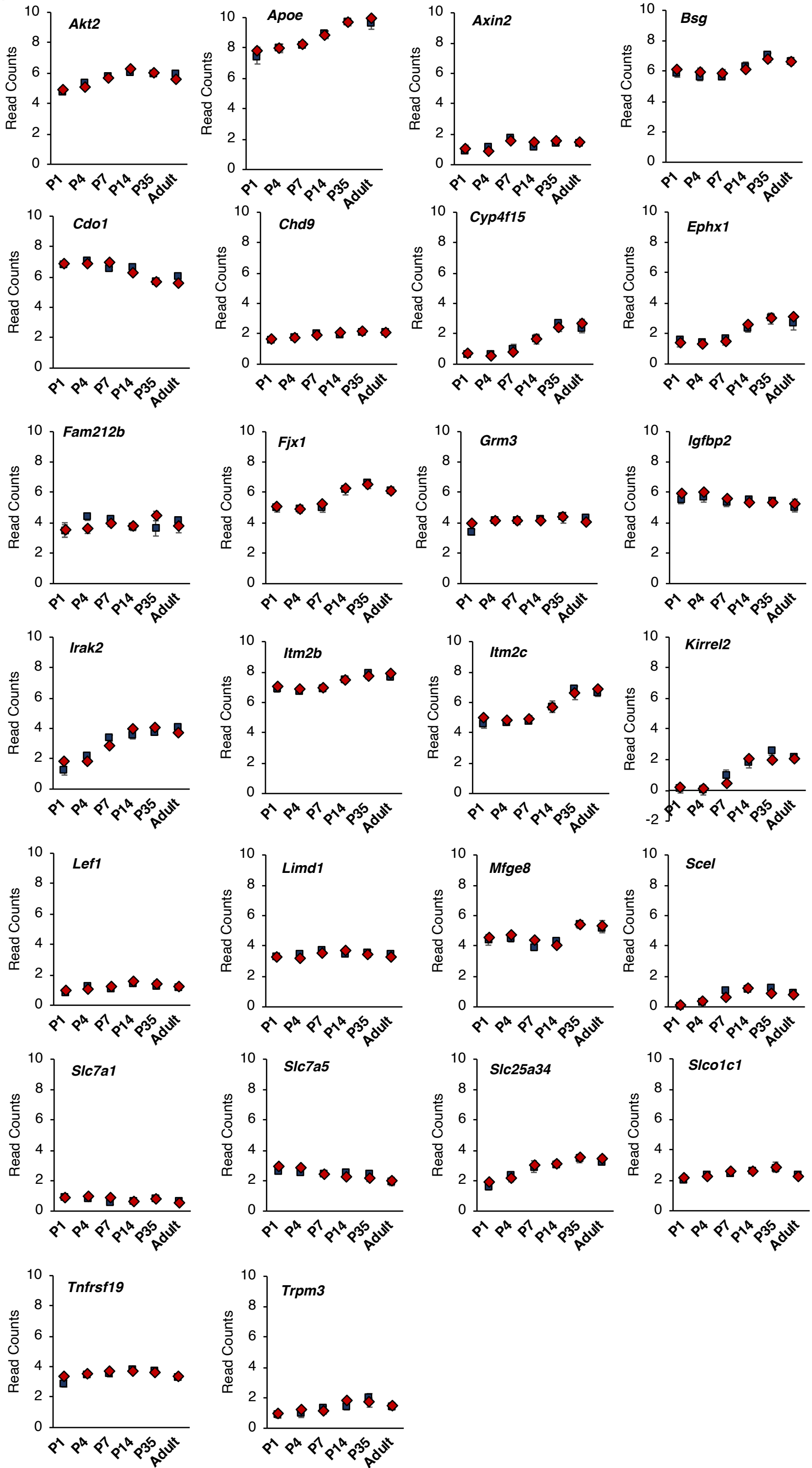

Supplemental Figure 9

TaqMan Gene Expression Assays	Gene Symbol	Dye	Assay ID
Glutamine Synthetase	Glul	FAM	Mm00725701_s1
Glial Fibrillary Acidic Protein	GFAP	FAM	Mm01253033_m1
RNA Binding Fox-1 Homolog 3	Rbfox3	FAM	Mm01248771_m1
Parvalbumin	Pvalb	FAM	Mm00443100_m1
Ly6/Neurotoxin 1	Lynx1	FAM	Mm01204957_g1
Estrogen Receptor 1	ESR1	FAM	Mm00433149_m1
Androgen Receptor	AR	FAM	Mm00442688_m1
Glutamate Ionotropic Receptor NMDA Type Subunit 2C	Grin2c	FAM	Mm00439180_m1
Progesterone Receptor	PGR	FAM	Mm00435628_m1
G protein-coupled Estrogen Receptor 1	GPER1	FAM	Mm02620446_s1
Actin Beta	Actb PL	VIC	Mm00607939_s1
Actin Beta	Actb PL	VIC	Mm02619580_g1

Supplemental Figure 10

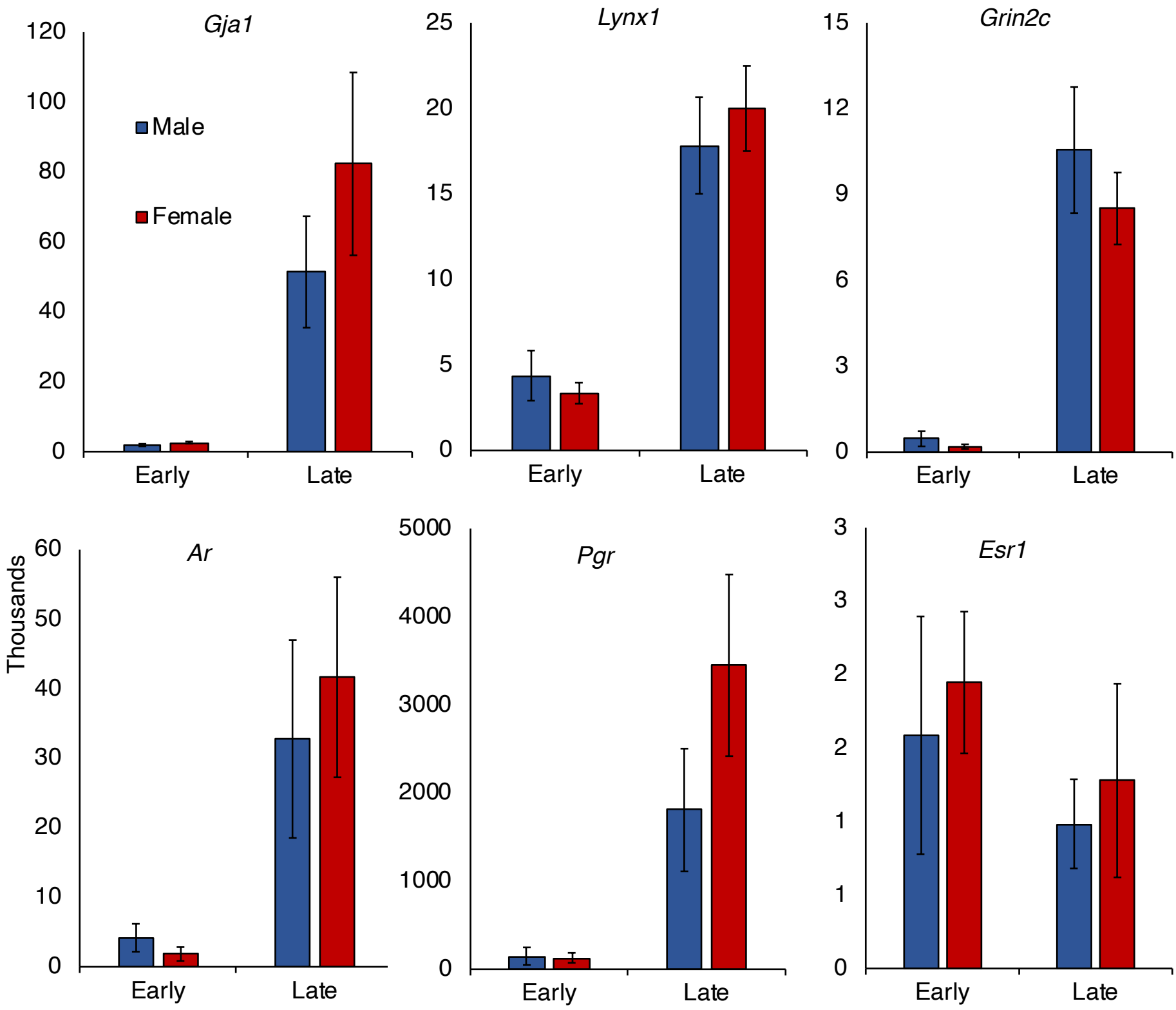

Q-RT-PCR validation of gene expression levels between early (P1-P7) and late timepoints (P14-Adult). Expressed as fold change

Supplemental Figure 11

	1	2	3	4	5	6	7	8	9	10	11	12
1. Gja1 Fold Change	1											
2. Gja1 RPKM	**0.56****	1										
3. Lynx1 Fold Change	0.48**	0.76**	1									
4. Lynx1 RPKM	0.46**	0.87**	**0.84***	1								
5. Esr1 Fold Change	-0.12	-0.02	0.08	0.08	1							
6. Esr1 RPKM	-0.01	-0.07	-0.15	-0.04	**0.39****	1						
7. Ar Fold Change	0.38**	0.51**	0.76**	0.53**	0.29**	-0.13	1					
8. Ar RPKM	0.47**	0.78**	0.91**	0.89**	0.46	-0.18	**0.75****	1				
9. Grin2c Fold Change	0.68**	0.68**	0.50**	0.63**	-0.28*	-0.07	0.18	0.56**	1			
10. Grin2c RPKM	0.53**	0.88**	0.77**	0.89**	-0.03	-0.14	0.48**	0.80**	**0.76****	1		
11. Pgr Fold Change	0.42**	0.53**	0.78**	0.57**	0.24	-0.08	0.96**	0.77**	0.22	0.51**	1	
12. Pgr RPKM	0.43**	0.76**	0.77**	0.83**	0.09	0.11	0.57**	0.84**	0.49**	0.70**	**0.61****	1

*** Correlation significant where $p < 0.05$ (2-tailed)**
**** Correlation significant where $p < 0.01$ (2-tailed)**

Correlation Table. Pearson correlations between Q-RT-PCR (fold change) validation of gene expression levels in TRAP samples and RPKM levels from TRAP-RNASeq.

Supplemental Figure 12

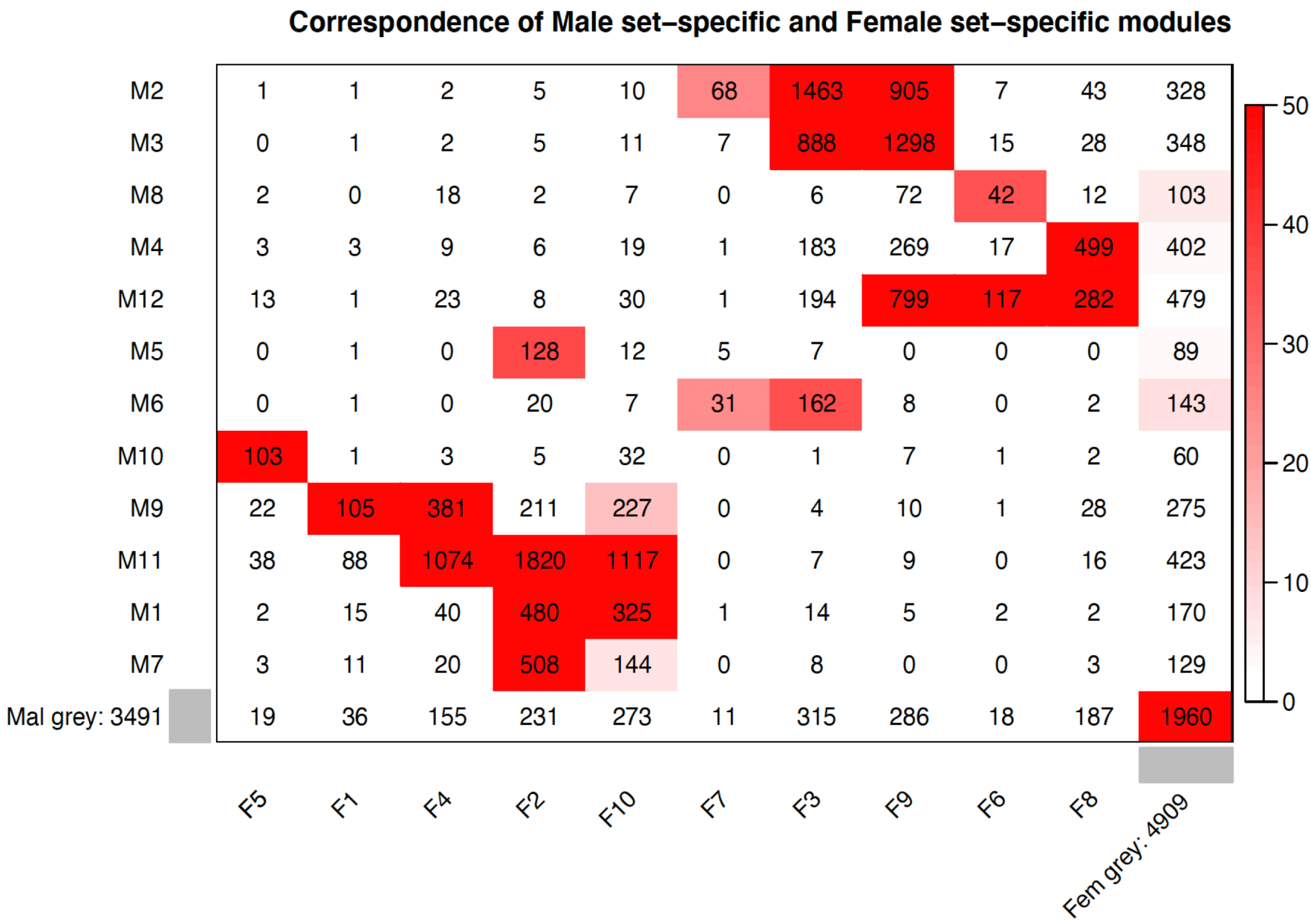

Supplemental Figure 12. Contingency table of the male modules (rows) and female modules (columns). The module color, and the total number of genes in the module label both the rows and the columns. Numbers within the table represent the counts of genes in the intersection of the corresponding row and column module. The table is color-coded by the $-\log_{10}$ of the Bonferroni corrected Fisher exact test p value (legend on then right).